To appear ApJ, 20May2004

A Catalog of Spectroscopically Identified White Dwarf Stars in the First Data Release of the Sloan Digital Sky Survey

S. J. Kleinman[1], Hugh C. Harris[2], Daniel J. Eisenstein[3], James Liebert[3], Atsuko Nitta[1], Jurek Krzesiński[1,4], Jeffrey A. Munn[2], Conard C. Dahn[2], Suzanne L. Hawley[5], Jeffrey R. Pier[2], Gary Schmidt[3], Nicole M. Silvestri[5], J. Allyn Smith[6,7], Paula Szkody[5], Michael A. Strauss[8], G. R. Knapp[8], Matthew J. Collinge[8], A. S. Mukadam[9], D. Koester[10], Alan Uomoto[11,12], D. J. Schlegel[8], Scott F. Anderson[5], J. Brinkmann[1], D.Q. Lamb[13], Donald P. Schneider[14], and Donald G. York[13]

ABSTRACT

We present the full spectroscopic white dwarf and hot subdwarf sample from the SDSS first data release, DR1. We find 2551 white dwarf stars of various types, 240 hot subdwarf stars, and an additional 144 objects we have identified as uncertain white dwarf stars. Of the white dwarf stars, 1888 are non-magnetic DA types and 171, non-magnetic DBs. The remaining (492) objects consist of all

[1]New Mexico St. Univ., Apache Pt. Observatory, PO Box 59 Sunspot, NM 88349: sjnk@apo.nmsu.edu.

[2]U.S. Naval Observatory, PO Box 1149, Flagstaff, AZ 86002.

[3]Steward Observatory, Univ. of Arizona, 933 N. Cherry Ave., Tucson, AZ 85721.

[4]Mt. Suhora Observatory, Cracow Pedgagogical Univ., ul. Podchorążych 2, 30–084 Cracow, Poland.

[5]Dept. of Astronomy, Univ. of Washington, Box 351580, Seattle, WA 98195.

[6]Los Alamos Natl. Lab., NIS-4 MS-D448, Los Alamos, NM 87545.

[7]Dept. Of Physics and Astronomy, Univ. of Wyoming, PO Box 3905, Laramie, WY 82071.

[8]Princeton Univ. Observatory, Princeton, NJ, 08544.

[9]Dept. of Astronomy, Univ. of Texas, Austin, TX 78712.

[10]Institut für Theoretische Physik und Astrophysik Universität Kiel, 24098 Kiel, Germany.

[11]Dept. of Physics and Astronomy, John Hopkins Univ., 3400 N. Charles St., Baltimore, MD, 21218.

[12]Carnegie Observatories, 813 Santa Barbara St., Pasadena, CA, 91101.

[13]Dept. of Astronomy and Astrophysics, Univ. of Chicago, 5640 S. Ellis Ave., Chicago, IL, 60637.

[14]Dept. of Astronomy and Astrophysics, Penn. St. Univ., University Park, PA, 16802.

different types of white dwarf stars: DO, DQ, DC, DH, DZ, hybrid stars like DAB, etc., and those with non-degenerate companions. We fit the DA and DB spectra with a grid of models to determine the T_{eff} and $\log g$ for each object. For all objects, we provide coordinates, proper motions, SDSS photometric magnitudes, and enough information to retrieve the spectrum/image from the SDSS public database. This catalog nearly doubles the known sample of spectroscopically-identified white dwarf stars. In the DR1 imaged area of the sky, we increase the known sample of white dwarf stars by a factor of 8.5. We also comment on several particularly interesting objects in this sample.

Subject headings:

1. Introduction

The Sloan Digital Sky Survey (SDSS: York et al. 2000) is a continuing imaging and spectroscopic survey of some seven to ten thousand square degrees in the north Galactic cap. Although its main focus is extra-galactic, there are many Galactic spin-off projects resulting from the survey. The SDSS's principal science objectives focus on obtaining redshifts of distant galaxies and quasars by first imaging the sky in 5 passbands, then selecting potential targets for spectroscopic follow-up based on the 5-band photometry. This spectroscopic selection process is referred to as "targeting" and many different targeting categories, each with different criteria and priorities, are used to fill all the fibers available on each 640-fiber spectroscopic plate. Where there are not enough primary targets (ie., galaxies, QSOs, etc.) to fill a given plate, the lower priority targeting categories (which include various stellar and serendipity categories) get to allocate fibers. SDSS obtained spectra are of high enough quality to allow accurate object and line identifications well beyond those necessary for redshift determinations. We thus end up with high-quality stellar spectra from objects directly targeted as interesting Galactic objects as well as those thought to be, but which ultimately were not, extra-Galactic objects.

Complementary to Harris et al. (2003) which presented white dwarf stars from a sample of early SDSS data, this paper reports on the white dwarf stars found in the spectroscopic data contained within the SDSS Data Release 1 (Abazajian et al. 2003, DR1: see also http://www.sdss.org/dr1). In a 190 deg^2 area of sky, Harris et al. (2003) found 260 white dwarf stars. In an area of sky 7.15 times larger, we find a factor of 9.85 more white dwarf stars, or an increased density of approximately 38% compared to that of Harris et al. (2003). We suspect this difference is simply due to random fluctuations in how we target and acquire white dwarf spectra in the SDSS. QSO target selection code changes, for example, can have significant effects on the ultimate yield of SDSS white dwarf spectra.

Since the DR1 spectroscopic coverage on the sky contains the area analyzed in Harris et al. (2003), all those stars are included here, although perhaps with a different spectrum than was analyzed in that work. The white dwarf sample presented here is not meant to be a statistically complete or even well-defined sample of white dwarf stars; it merely represents the white dwarf stars that happen to have spectra in DR1. There are undoubtedly many more white dwarf stars contained within DR1 for which we only have photometry. We make no attempt to report on those stars here (except see the Appendix for data on previously known white dwarf stars in DR1 for which we do not have spectra).

We also include spectra for hot subdwarf stars, the sdB and sdO stars, since they overlap the hot white dwarf stars in color-color space and need to be identified in order to find the white dwarf stars (besides being interesting in their own right, of course). For the broader context of white dwarf stars in the SDSS and particular notes of some unusual objects, see the Harris et al. (2003) paper and the earlier simulations of Fan (1999) who discusses where the white dwarf stars should appear in the SDSS photometric color space.

The SDSS spectra are well-described in Stoughton et al. (2002) and Abazajian et al. (2003). Briefly, they cover a wavelength range of approximately 3800–9200Å with a resolution $\sim$ 1800 and are spectrophotometrically calibrated to within about 10% on average. The average S/N of a g=20.2 spectrum is $\sim$ 4 per pixel and the redshift accuracy is of order 30 km s^{-1}, as determined for the SDSS galaxy sample.

The McCook & Sion (1999) catalog lists 2249 white dwarf stars while the online updates (at http://www.astronomy.villanova.edu/WDCatalog/index.htm) now include a total of 3066 white dwarf stars (as of June, 2003), some of which are included in the first SDSS white dwarf catalog paper by Harris et al. (2003). Here, we present 2551 certain white dwarf stars, 240 hot subdwarf stars, and another 144 possible, but uncertain white dwarf and hot subdwarf stars from the 1360 deg^2 of DR1. We find 108 of our white dwarf stars are already present in the McCook & Sion (1999) catalog. We present a more complete description of the overlap between the two catalogs in the Appendix.

Another comprehensive spectroscopic survey, the 2dF QSO Redshift Survey (Boyle et al. 2000), has also produced a sizeable catalog of white dwarf stars (Vennes et al. 2002). The 2dF survey went a bit deeper than the SDSS, but covered a smaller solid angle: 740 deg^2 with $18.4 \leq B \leq 21.0$ (Vennes et al. 2002). Their results include 942 spectroscopically-identified DA white dwarf stars, providing another large increase in the number of known white dwarf stars.

2. Object Identification

The spectroscopic reduction pipeline of the SDSS does not classify stellar objects with much detail, so we cannot rely on the standard reduction output to accurately select out white dwarf and subdwarf stars from the myriad of stellar (and non-stellar) spectra available. We thus have to identify a set candidate white dwarf spectra, then manually examine each spectrum to determine the object's classification.

The first task, then, is to identify the candidate spectra. While there is a specific white dwarf targeting category, the relative priority of this category is low and we use it mainly to search for the potentially coolest of the white dwarf stars (Harris et al. 2001). We thus cannot view the white dwarf targeting category as anywhere near a complete sample of candidate white dwarf spectra and therefore rely mainly on color and proper motion information to choose our candidates. The resulting candidate spectra were targeted by a variety of SDSS targeting categories. Table 1 summarizes the SDSS targeting criteria that were used to obtain each of our identified white dwarf and hot subdwarf spectra. Note, this table just lists the targeting category that was actually responsible for the fiber allocation; it may well be that an object matched the criteria of multiple target selection categories, but was ultimately allocated a fiber by only one of them. Blanton et al. (2003) and Stoughton et al. (2002) give more details on the targeting process and provide a description of the different targeting categories.

The targeting categories listed in Table 1: GALAXY, QSO, and STAR_WHITE_DWARF are self-explanatory; ROSAT is for a variety of ROSAT (Voges et al. 1999) sources as thoroughly described in Anderson et al. (2003); SERENDIPITY has several sub-categories: MANUAL are targets manually selected and assigned a fiber for any variety of reasons, DISTANT looks for unresolved sources that are distant *from the stellar locus*: either very red in $(g - r)$ or very blue in $(r - i)$, and BLUE is for objects that are particularly blue in $(u - g)$; the STAR category also has several sub-categories: BHB are potential blue horizontal branch stars while CATY_VAR are potential cataclysmic variables; QA objects are purposefully-selected targets which have been observed on another plate and whose repeat observations are used for quality assurance purposes; and finally the HOT_STD category represents hot standard stars used for spectrophotometric calibrations. As Table 1 shows, only a very small percentage of objects were targeted directly as potential white dwarf stars and most are simply selected as blue objects from the SERENDIPITY, QSO, and HOT_STD categories. Richards et al. (2002) discuss the SDSS QSO selection algorithms and describe the overlap in QSO and white dwarf color-color space in the SDSS.

All of the 13 DR1 DOs, however, were targeted by the HOT_STD algorithm. Since the HOT_STD spectra are used for spectrophotometric calibration and the space density of these objects is relatively low, the category is allocated fibers with a very high priority. Thus, the DO, along with the hot DA and subdwarf, sample from the SDSS should be highly complete for isolated stars[1], while the completeness of the rest of the white dwarf subgroups is not as high and difficult, although theoretically possible, to calculate. The HOT_STD algorithm picks isolated stars with dereddened $(u-g)$ and $(g-r)$ colors between –1.5 and 0 mag and g roughly between 14 and 19 mag. Since we have SDSS color information and USNO-derived proper motions (Munn et al. 2003) for every SDSS-detected photometric object, and we know which ones were allocated a spectroscopic fiber by what algorithm, and we know which of these ended up being which type of white dwarf star, we have a hope of untangling the complicated selection function and estimating a complete white dwarf luminosity function in the area of the SDSS. We leave that project, however, to future work.

Despite their relative structural and evolutionary simplicity, white dwarf stars are actually quite varied as a group, and thus we used several different criteria to try to assemble a list of all SDSS white dwarf candidate spectra. Because we knew the task of combing through the resultant spectra was going to be time-consuming, we prepared the list of candidates in the summer of 2002, before the the final DR1 photometric reductions were complete and before the final DR1 spectroscopic sample had been settled upon. Therefore, all photometric selections were made on an earlier version of the photometric pipeline than what ultimately appeared in DR1 and our candidate list was different from that which we would get now were we to repeat the process on the final DR1 data set. The differences in the photometry due to the changes in the pipeline are mostly minor and our selection criteria were purposefully broader than likely necessary, so we expect very few (if any) true white dwarf stars were missed by photometric criteria. Since the final selection of exactly which spectra would appear in DR1 was not ready at the time of our candidate selection, we sometimes looked at a spectrum for an object that was ultimately included in DR1 but with a different spectrum taken at a different time than the one we analyzed. In these cases, we have made the cross-assignment of our identification to the new spectrum. We looked at many of the repeat spectra by eye and found identification changes only in cases where one spectrum had a significantly higher signal-to-noise ratio (S/N) than the other.

Table 2 summarizes the selection criteria we used to generate our white dwarf candidate list. The criteria are written with the same field/quantity names as are available in the SDSS database so the search can be directly repeated. These criteria resulted in 10,800 spectra of 9,400 unique objects. About two thirds of these objects were ultimately included in DR1.

---

[1]Harris et al. (2003) found 90% completeness in a smaller area of the sky for white dwarf stars with $T_{\rm eff} >$ 22000K and $15 < g < 19$.

Once we had our candidate list, we manually inspected each spectrum and made a coarse identification. We then sorted the results into different categories of white dwarf stars and non-white dwarf stars and fit the DA and DB spectra with models for $\log g$ and $T_{\rm eff}$ determinations (see below). We did not fit the spectra of the non-DA/DB white dwarf stars due to their inherent increased model complexity. We note that nine of the white dwarf + main sequence binary systems reported in Raymond et al. (2003) did not make any of our selection cuts, although we have manually added them to our tables for completeness.

Our spectroscopic identifications follow the convention of Sion et al. (1983). Briefly, DA, DB, and DO stars are white dwarf stars which show lines of H Balmer series, HeI, and HeII respectively. DQ stars show C lines; DZ stars have metal lines; DH stars show signs of magnetic fields; and DC stars show continuous spectra, showing no discernible spectral features. Hybrid stars are indicated with the dominant component's symbol first; the secondary, later. For example, a DAB star is one with dominant H lines, but that shows some HeI lines as well.

3. Human Identification Complexities

There were many complications in identifying some classes of white dwarf stars from our candidate list. Low S/N spectra (typical for magnitude 20, or greater, objects) pose a classification problem as noise can make the observed hydrogen or helium lines appear broader than they really are. Where the widths of the lines were judged to be likely broad, but uncertain, we checked as to whether a proper motion was detected above about 15 mas yr^{-1}. If there was such a motion, we included the star in the DA list; if not, it was called DA:, the *:* suffix indicating an uncertain identification, and placed in the uncertain white dwarf list. We also used the $(u-g)$ and $(g-r)$ colors to help separate the main sequence A and F stars from the DA and sdB stars. Main sequence A and F stars (and even some horizontal branch stars) may appear to have similar line widths as sdB stars but very different $(u-g)$ colors (due to the larger Balmer jump).

Very hot stars pose problems because they generally have weak lines and are likely too distant to have a detectable proper motion if they are white dwarf stars. These objects might be classified DA: or sdO: based on spectral features judged to be possibly present.

The cool DB stars also pose a special problem. The line widths of He I in these stars become quite narrow and similar to those of the sdO (or He-sdB) stars. The latter, however, have substantially stronger He I 4388Å relative to He I 4471Å than do the true DBs. We therefore relied on this criterion to make the judgment, but if the spectrum was poor and line strengths difficult to judge, we used the detection of a meaningful proper motion (> 15 mas yr^{-1}) as sufficient to classify the star a DB. Otherwise, we judged it based on the appearance of the low S/N He I lines to be either DB: or sdO:. The colors are, unfortunately, similar for these two types.

The proper identification of featureless spectra can potentially be either a DC white dwarf or an extra-galactic object with weak or no features (i.e., a BL Lac object). Unfortunately, these two classes can overlap considerably in color. The designation was BL Lac if the source had a counterpart in the FIRST (Becker, White, & Helfand 1995) radio or ROSAT (Voges et al. 1999) X-ray surveys, since cool white dwarf stars are not radio or X-ray sources. Here again, we used the detection of a meaningful proper motion as a valid basis for choosing the DC classification. Anderson et al. (2003) also discuss some of the difficulties and techniques in identifying featureless SDSS spectra.

There were a number of cases where the proper motion and colors indicated that the object is a white dwarf, but the spectral type is uncertain due to uncertain spectral features seen. We used the identification WDDB:, for example, if possible He I lines were judged to be in the spectrum, the *WD* indicating a certain white dwarf star and the *DB:* indicating it might be a DB. Likewise, this ambiguity could occur for hybrid spectra. For example, a DB spectrum showing a possible but not definite Hα line would be denoted DBA:. (Note that the Balmer decrement is very steep in DBA stars — often only Hα is detectable.)

Figures 1 and 2 show the resulting ugr and gri SDSS color-color diagrams for identified white dwarf objects. We did not plot any objects that have magnitudes that are flagged as bad photometry by the SDSS pipeline (see discussion below). The SDSS photometric system is well described by Stoughton et al. (2002), Smith et al. (2002), Hogg et al. (2001), Fukugita et al. (1996), and Gunn et al. (1998). The plotted colors are observed point-spread-function (PSF) magnitudes from the *best* version of the SDSS photometric database[2], with full extinction/reddening corrections (Schlegel et al. 1998) applied to each object. Of course, it is not correct to apply the full reddening correction to every object since some will be close to us and in front of the dominant extinction sources. However, it is also not easy to determine exactly how much extinction is appropriate for each individual object. To be consistent with Harris et al. (2003), though, we chose to apply the full correction always (and indicate this in our colors/magnitudes with a subscript $_\circ$). Since most of our objects

---

[2]The SDSS photometric database includes two sets of data for each object. The *target* version is the original photometric detection reduced with whatever the current photometric software was at the time. This version represents what was used to determine spectroscopic target selection. The *best* version could be the same, or later, detection of the object reduced with the latest version of the photometric pipeline. Except when investigating targeting effects, the *best* sky version is usually the appropriate one to use.

are at high galactic latitudes, the extinction is often small, at any rate. Our color-color plots clearly show the separation of the hotter DAs from the more continuum-like DBs and DCs. The WDM points represent white dwarf stars with non-degenerate companions (see Raymond et al. 2003).

Some features seen in these plots cannot be interpreted as indicative of the white dwarf population at large. Since the SDSS spectroscopic targets are chosen based largely on color cuts in SDSS photometry, there are significant selection effects in our sample. However, it is nice to note the expected continuation of the identified subdwarf stars into the realm of the blue horizontal branch stars (between $(u - g)$ of ≈ 0.5 to 1.0) which demonstrates the arbitrary separation between the hot subdwarf and extended horizontal branch stars. These objects have colors which indicate temperatures intermediate between the traditional horizontal branch and the normal sdB stars.

4. The Tables

We present several tables of our spectroscopically identified SDSS white dwarf and subdwarf samples. Tables 3 and 4 list the DA and DB white dwarf stars, respectively, along with their model-fit $T_{\rm eff}$ and $\log g$ as described in the next section. These tables are ordered by fit temperature. Table 5 lists all the white dwarf and hot subdwarf stars we have identified, including the human-ID for each one (DA, DB, DQ, etc.). Finally, Table 6 lists all the objects that we are less certain of, but which could be white dwarf or hot subdwarf stars. The latter two tables are ordered by right ascension and declination. All our tables are also online at the SDSS DR1 value added catalog site: http:///www.sdss.org/dr1/products/value_added/wdcat/dr1/index.ht The online catalogs have links to the SDSS spectra and finder charts, as well as to plots detailing our model fits.

We do not separate the DCs, DQs, DHs, DZs, or binary white dwarf stars in these tables, but refer the interested reader to Harris et al. (2003) for a more general discussion of these other white dwarf subtypes, Schmidt et al. (2003) for a discussion of the magnetic white dwarf stars, Liebert et al. (2003a) for a discussion of white dwarf stars with carbon and oxygen lines, Raymond et al. (2003) for a discussion of white dwarf plus main sequence M star binaries, and Krzesinski et al. (2004) for a discussion of the SDSS DO white dwarf sample. Finally, Mukadam et al. (2004) describe the discovery of 32 new DAV (ZZ Ceti) pulsating white dwarf stars from our DA sample and include the many SDSS DAV candidates observed that were ultimately non-pulsators, and Nitta et al. (2004) discuss new DBV (V777 Her) pulsators resulting from the new DR1 DBs.

Each entry in the tables starts with the object's official SDSS name. The format of the name is SDSS JHHMMSS.ss+DDMMSS.s where the HHMMSS.ss is the truncated (not rounded) hours (HH), minutes (MM), and seconds (SS.ss) from the SDSS J2000 right ascension and the +DDMMSS.s is the truncated declination in degrees, minutes, and seconds. Each object should be referred to by these names. We also provide the right ascension and declination in decimal degrees, as that is a convenient format for use in SDSS databases. SDSS astrometry is thoroughly discussed in Pier et al. (2003) and reported positions are good to less than 0.1" rms. Since the SDSS coordinates are all reported for equinox 2000.0 at the epoch of the *best* imaging observations, we also include this epoch in our general catalogs, Tables 5 and 6. In addition, we list the SDSS plate, MJD, and fiberID, needed to uniquely obtain the SDSS spectrum from the DR1 data archive server (http://das.sdss.org/DR1-cgi-bin/DAS). The plate number describes the pre-drilled plate of 640 fibers with which each object was observed. The fiberID details which of the 640 fibers gathered each particular spectrum and the MJD is the SDSS-modified Julian date on which the data were taken. Next are the *ugriz* PSF magnitudes and uncertainties. along with the final median S/N squared per pixel of the spectrum from the DR1 *best* database. We precede each magnitude that is flagged by the SDSS pipeline as questionable with an *. Table 7 lists the photometric flags we checked along with a brief description of each flag. See Stoughton et al. (2002) and Abazajian et al. (2003) for more details of all SDSS outputs.

The DR1 database contains a proper motion, where measured, for each photometric object, but the proper motions we present here are not those from the SDSS database. Instead, proper motions have been measured with the following procedure. First, we matched each of our objects against the USNO–B1.0 catalog (Monet et al. 2003) by finding objects in USNO–B within 1" of each SDSS position at the epoch of the SDSS imaging scan. Next, we extracted the position of each detection of the matching object from USNO–B, giving up to five measurements and epochs on the five sky survey plates included in USNO–B. We corrected each of these USNO–B positions for systematic errors by subtracting the mean difference between the SDSS and USNO–B positions for the nearest 100 galaxies in the magnitude range $17 < g < 19.5$. Finally, we recalculated the proper motion using the SDSS position plus all (up to five) USNO–B positions. We used a weighted linear solution, assuming errors of 45 mas for the SDSS position and 120 mas for each sky survey position in each coordinate for determining the relative weights in the solution. This procedure improves proper motions by a significant amount and is described more fully by Munn et al. (2003). The motions have rms errors of 3–5 mas yr^{-1}in each coordinate. We generally consider any proper motions less than 12 mas yr^{-1}as not significant.

Finally, each table also has the extinction in the SDSS g filter, A_g, as stored in the SDSS photometric database. These values use the reddening maps as presented in Schlegel et al.

(1998). Table 8 lists the multiplicative factors for converting A_g into the extinctions in the other SDSS filters, as described by Schlegel et al. (1998) and Stoughton et al. (2002). We also include various entries in the *Notes* column to highlight certain objects or indicate the results of our human checks of the computer fits (described below).

The DA and DB tables also list our model-fit-determined $T_{\rm eff}$ and $\log g$ and their corresponding uncertainties along with the χ^2 of the best fit. Following the $T_{\rm eff}$ and $\log g$ determinations is the ASCII ID for each spectrum from our fitting code. The format is simply DA or DB followed by the $T_{\rm eff}$ subtype (50400K/$T_{\rm eff}$) and the $\log g$, separated by an underscore. The *CH:* prefix and colon suffix are quality assessment checks which are discussed in the next section. Where our check on the auto fitting deemed the fit invalid, we replace the fit parameters with zeroes and the fit ID with *N/A*. The combined and uncertain white dwarf tables list only the human ID for each object, since we only fit models to the DA and DB stars. A colon in the human ID means the identification is uncertain, but only the modifier immediately before the colon is deemed uncertain. For example, DA9: refers to a star that we consider to be a DA, but which we think is a DA9 subtype. (Most of our human IDs, however, do not include subtypes.)

5. Model Fitting

We fit each human-identified DA and DB spectrum to theoretical models from Detlev Koester to determine their temperatures and surface gravities. Koester's models are described in Finley, Koester, & Basri (1997), although we received an updated grid at the time we started our analysis. One change in the current models from those described in Finley et al. (1997) is the use of the now-standard ML2/α = 0.6 convection model. The hydrogen atmosphere models range in $T_{\rm eff}$ from 6000 to 100,000 K and in $\log g$ from 5 to 9. The helium atmospheres range in $T_{\rm eff}$ from 10,000 to 40,000 K and in $\log g$ from 7 to 9. Our procedure is to measure the χ^2 statistic on the difference between the observed spectra and the models, using the quoted errors from the SDSS spectroscopic pipeline. For DA stars, we use only the wavelength range 3870Å to 7000Å; for DB stars, we use 3870Å to 5400Å(for reasons described below). We exclude pixels that are flagged by the spectroscopic pipeline in the "AND" mask (meaning that the pixel was masked in all exposures) with the bits `0x1fff0000`. This mask includes all single-pixel failure modes. In addition, we visually inspected all cases in which one or both cameras of the spectrograph were flagged with the full-chip mask bits `0x1cf`. The results of the visual inspection are indicated in the *Notes* section of the tables, with "1" and "2" meaning trustworthy and untrustworthy, respectively.

The SDSS spectrographs have a typical instrumental dispersion of about 170 km s^{-1}

FWHM. Because this is considerably less than the typical line widths in white dwarf stars, smoothing the models to the instrumental resolution (or not) does not affect the fits much. We have not smoothed the models for the fits presented. The error introduced by this for DAs is less than 1% in temperature and generally negligible (0.02 dex) in $\log g$; however, at temperature below 10^4K (where our input model grid has systematic errors anyway), our gravities are biased high by 0.1–0.2 dex. For DBs, the effects on temperatures are small (less than 3%), but the gravities are biased high by 0.1 dex for temperatures below 20,000K. We plan to include the fits with instrumental dispersion in future samples which will be available at the SDSS value-added catalog URL given earlier.

Because of unknown reddening and the desire to insulate the procedure from spectrophotometry errors, we permit the fit the freedom to re-flux the models according to a low-order polynomial. This is done efficiently by performing the χ^2 fit as a linear least squares optimization to a set of vectors defined by the model spectrum and the model spectrum multiplied by a series of smooth basis functions. We use the first seven Chebychev polynomials (with the first being a constant) in linear wavelength as our refluxing basis. By using the minimum in χ^2 for this 7-dimensional optimization as our basis for comparison between models, we are effectively marginalizing over the refluxing parameters. The shape of the Cardelli, Clayton, & Mathis (1989) extinction curve over this octave in wavelength is extremely well modeled by a 6th-order polynomial, and so our procedure fully marginalizes over reddening uncertainties.

Due to the near degeneracies in the line strengths and profiles of white dwarf stars, we supplement the spectroscopic fitting with additional information from the SDSS photometry. Each model is convolved with the SDSS filter curves to yield predicted colors. The SDSS photometric zeropoints nearly but not exactly satisfy the AB convention (see Stoughton et al. 2002; Abazajian et al. 2003). We correct the photometric zeropoints from the AB system to the SDSS system by $u(AB) = u(SDSS) - 0.04$ and -0.01, 0, 0.015, and 0.03 for g, r, i, and z, respectively. These corrections are approximate and still subject to change. We then construct the χ^2 statistic for the difference between the observed colors and the predicted colors using the quoted errors in the five bands, with a systematic floor of 0.007 mag added in quadrature (0.015 mag in u and 0.010 mag in z). To account for reddening, we apply a baseline correction of 50% of the Schlegel et al. (1998) reddening map and then marginalize over the reddening direction in color space (assuming $R_V = 3.1$) with a 1–σ prior of 50% of the predicted reddening. We then forbid reddening values less than zero and penalize values above the Schlegel et al. (1998) value with a prior of $90\% \pm 10\%$ of the predicted value (thereby yielding a continuous χ^2 distribution). In other words, we adopt a reddening prior of 0.5 ± 0.5 of the predicted value with a steeper wall at unity and a sharp cutoff at zero. Clearly, this is an approximation, but our primary goal is to pick the correct local minimum in degenerate cases. We sum the spectroscopic and photometric χ^2 with equal weight.

Having computed the χ^2 for each model, we estimate the best fit and errors in two ways: 1) Use the lowest χ^2 model with a quadratic fit to the neighboring points to find the interpolated minimum and errors, and 2) Convert the χ^2 into a Gaussian likelihood and simply find the moments of this distribution, assuming a uniform metric in inverse temperature and log g. The fit values presented in the tables are from the likelihood moments.

In the case of multiple near-degenerate minima, the likelihood estimate will try to split the difference (and greatly increase the errors), while the global minimum will make a somewhat arbitrary choice. Hence, we monitor the difference between these two estimates as a way to find cases with multiple minima. Inspection of near-degenerate cases suggests that the likelihood error range includes both minima, but the reader should be aware that the quoted mean fit isn't necessarily near one of the minima.

Our fitting procedure relies upon a somewhat coarse set of models between which we interpolate a fine grid. We have identified two negative consequences of this procedure. First, models that fit to gravities near the edge of the grid, in particular the upper bound at $\log g = 9$, are incorrectly thrown against the boundary and given very small errors. This anomaly sets in at $\log g \gtrsim 8.8$, and any quoted numbers above this should be viewed only as indications of high gravity rather than an accurate fit. Second, for DA stars of very high signal-to-noise ratio, our model grid is simply not fine enough. Essentially we are estimating the quadratic shape of the χ^2 distribution from points far from the minimum. We expect that this leads to some lack of accuracy and an underestimate of errors. This problem seems to occur when the errors in temperature fall below 1% of the temperature itself. Future versions of our model fitting will attempt to address these problems.

Since the release of DR1 (Abazajian et al. 2003), Tremonti et al. (2003) have made significant improvements to the spectrophotometry of the SDSS pipeline. These improvements will be available in the next public data release, DR2, but having them at our disposal now, we have used these spectra for our fits rather than the as-released DR1 versions. Our tests (described below) of internal errors of repeat spectra reduced with both pipelines, however, give us confidence that our results are still representative of the publicly-available DR1 spectra.

The fitting code performs two levels of checks to monitor the quality of its fits. We mark the most severe problems with a *CH:* (which stands for "Check") at the start of the ASCII identification output of the code (included in the DA and DB tables). The *CH:* indicates that the code could not find any satisfactory fit, but it reports the best it had. These checks can be triggered for several reasons: the spectrum had too many masked pixels, the reduced

χ^2 of the best fit was too high or too similar between the DA and DB best fits, there were two minima in the likelihood fit surface, the S/N of the fit spectrum was too low, and/or the photometric colors disagreed significantly from the best fit. We looked at each of the *CH:* cases by eye and determined whether or not the fit was reasonable despite the program's complaints. Where the fit was found reasonable, we include fit parameters and a *1* in the *Notes* column; where not, we do not include any of the fit parameters and add a *2* in the *Notes* column.

Other, less severe trouble indicators are marked with a *:* appended to the program's ASCII identification. In general, however, we find no evidence that the identifications flagged with colons are any worse relative to their quoted errors than are the non-colon objects. The reasons for triggering these warnings are similar to those for the *CH:*, but less severe: the reduced χ^2 was marginal (between 1.2 and 1.5) or too good χ^2 (indicating perhaps a loss of signal in the spectrum), the χ^2 of both the best DA and DB fits were marginally similar, the S/N of the spectrum was moderately low, a DB fit log g was pegged to an endpoint of the DB grid, the colors disagreed moderately with those predicted from the best fit, the necessary refluxing was too large, and/or an improbable reddening value was needed.

Two sample fit DA output plots are shown in Figures 3 and 4. The fit parameters are similar for the two objects, but the first has a g magnitude of 16.9, while the second object is g = 20.5. Figure 5 is for a g = 18.9 DB. The top half of these plots shows the fit contours in log g – subtype space, with subtype being the usual $\mathrm{T_{eff}}$ expressed in units of $50400\mathrm{K}/\mathrm{T_{eff}}$ (Sion et al. 1983). The likelihood contours are at 1, 2, 3, 5, and 10-σ (i.e. $\Delta\chi^2 = 2.3, 6.2, 11.8, 29$, and 105 for the two-dimensional distribution). The bottom panels show various zooms of the fit plotted with the spectrum itself (reddened as observed). The dashed line fit is the fit without the refluxing (and without any reddening); the solid line fit is the adopted refluxed fit.

Visual inspection suggests that the model fitting procedure works well for DAs. The inclusion of the photometry usually breaks the line-degeneracies between hot and cold DAs. We find that at temperatures below $10,000$ K, the fitted gravities significantly exceed $\log g =$ 8. We believe this may be a failing of the input models (see next section), although in the extreme limit of $\log g = 9$, our procedures encounter the systematic problem listed above. We have made no attempt to treat DA+M binaries or DAe emission line contamination properly, so fits to such objects should not be trusted. Binaries are usually found because of their severe photometric residuals in the z band and the absorption bands in the red part of the spectrum. Subdwarf B stars are generally recovered as low gravity objects, but we have not attempted to fit the diversity of hydrogen and helium lines that are found in these stars. Thus, we only present fitted $\mathrm{T_{eff}}$ and log g values for what we think are single DA and DB stars.

DB white dwarf stars are more difficult to fit because above about 18,000K, the line strengths depend more weakly on temperature. Small systematic errors in the observations or the models appear to cause large shifts in the fitted temperatures that significantly exceed the formal errors. The photometry provides an additional source of information on the temperatures, but this can sometimes be ambiguous because temperature and reddening have similar effects on the colors. We note that the prior on the reddening is tied to the predicted extinction, and therefore stars in high extinction regions will be less constrained by the photometry. If this leads to a bias, the magnitude of that bias would be galactic-latitude dependent. In short, while the fitting pipeline appears to be correctly finding the hot DBs, we do not believe that our detailed fits to the hot DBs are reliable. We have, however, begun a program to look at the hotter DBs for variability and to date, have found two out of four well-observed candidates to be variables (Nitta et al. 2004), suggesting our hot DB fits are at least indicative.

We found that the fitted gravities in cooler DBs tend to be substantially higher than the conventional value of $\log g = 8$. However, we find that this result is quite sensitive to whether the lines between 5400Å and 7000Å are included in the fit. This may indicate subtle errors in the models, at least in certain lines. We have not addressed this source of systematic error save by choosing to restrict our DB fits to the spectrum shortward of 5400Å.

The values of the spectroscopic χ^2 are often quite close to one per degree of freedom even in cases of good S/N. This is very encouraging, as it indicates the quoted errors from the spectroscopic pipeline do properly represent the pixel-to-pixel noise in the spectra. However, the errors we find from the standard χ^2 methods are rather small. To investigate the validity of our errors, we found 265 of our white dwarf spectra (242 DAs, 23 DBs) that had repeat spectra taken by the SDSS and which our fitting avoided "Checks" on both fits. In all cases, these repeat spectra are separate exposures taken on different nights than the first observation. Most are simply repluggings of the same plate (meaning the relation between optical fibers and plug holes have been permuted) and hence share the same calibration stars but typically illuminate different detector pixels. We fit each of the repeat spectra and compared with the results from the original spectra fits, using the same photometry in both cases. In detail, the "second-epoch" spectra we used in this comparison were reduced with the DR1 pipeline, rather than the DR2 pipeline that we used for our primary set of stars. The good agreement we describe below demonstrates that the fits are reasonably insensitive to continuum changes and fluxing errors.

Figure 6 shows the difference between the fitted temperatures divided by the quadrature summed uncertainties versus the same quantity for $\log g$ for the repeat DA and DB samples. The ellipses shown in these plots are the contours that should include 68%, 95%, and 99.7% of the points if the distributions were Gaussian and independent. The DA fit residual distribution is about 40% larger than the Gaussian predictions from the formal errors. There is some hint that the scatter in those stars where the formal errors are below 1% in temperature is slightly worse than the other stars. However, it is important to stress that 78% of the DAs have temperature differences less than 5%, and only 5 of the 242 changed temperature by more than 20% (at least 3 of these cases are jumps across the temperature degeneracy). The DB distribution is only about 10% larger than the Gaussian prediction, after excluding the one catastrophic outlier (in which a star jumped across the temperature degeneracy). We suspect, however, that this relative agreement is forced upon us by the photometric weighting in our fits and that our fitting probably is not as good as with the DAs. Clearly, systematic errors in the fitting procedure or in the theoretical models are not tested by the repeat spectra. In summary, though, we suspect our DA uncertainties are underestimated by roughly 40%, and probably a similar amount for the DB fits.

Figure 7 show the relative T_{eff} and absolute $\log g$ differences produced by our fitting routines versus those available in the literature for previously known DA stars. There are only 20 stars used in this comparison, but some have multiple literature fits which are all included. The solid squares represent literature fits based on Koester models (Koester et al. 2001; Homeier et al. 1998; Finley et al. 1997), the circles are based on Bergeron models (Bergeron et al. 1992a; Bergeron et al., 1994), and the asterisks are based on other models (Marsh et al. 1997; Vennes et al. 1997; Napiwotzki, Green, & Saffer 1999). The figure shows a good agreement for T_{eff} < 25,000K or so, with a systematic trend in our fits to overestimate T_{eff} when compared with literature values, increasing as T_{eff} increases to within 5% for T_{eff} <30,000, within 10% for T_{eff} < 60,000K, and increasing to as much as a 20% relative overestimate for our highest T_{eff} fit near 90,000K. The Bergeron and Koester literature fits agree with each other quite well, so our differences are probably due to our method of fitting, perhaps our use of refluxed continuum fits versus the traditional line profile fitting.

The $\log g$ plot shows reasonably good agreement in the T_{eff} range around 15,000 – 50,000K, but we tend again to overestimate (as much as 0.4) the quantity for stars much cooler and much hotter than that when compared to the literature fits. We discuss below possible problems to the model fits to cool stars, but our systematic increase in $\log g$ appears to be worse than that found by other investigators, although the sample of cool stars is small here. The general trend to both higher T_{eff} and $\log g$ with increasing T_{eff} makes some sense in that our code is trying to compensate for the higher T_{eff} by also increasing $\log g$ (or vice versa).

We regard this method of model fitting as reasonably accurate, but we cannot rule out the possibility of as much as 10% biases in the temperature scale as discussed above. The recent successes of Mukadam et al. (2004) in finding DAV pulsators and Nitta et al. (2004) in finding DBV pulsators based on our fit-determined parameters, and the theory that each instability strip is purely a function of log g and $T_{\rm eff}$, give us additional confidence the fits are reasonable. Indeed, our $T_{\rm eff}$ fits agree to within 5% to literature values for DAs with $T_{\rm eff}$ < 45,000K. Like all automated pipelines, outliers should be viewed with some suspicion; the fit and spectra of interesting cases should be checked by eye before investing telescope time on their further study. To facilitate these checks, we have made plots similar to Figures 3 through 5 available for all our DA and DB fits in the HTML version of our catalogs, available on the SDSS DR1 value added catalog web page at http:///www.sdss.org/dr1/products/value_added/wdcat/dr1/index.html.

6. Discussion

Figures 8 and 9 show $T_{\rm eff}$ and log g vs. $(u-i)_\circ$ for our DA and DB fits. The $T_{\rm eff}$ plot shows a nice correlation, as expected, between $T_{\rm eff}$ and color. The line in this plot comes from Bergeron et al. (1995) models convolved with the SDSS filters with no AB corrections made. The AB corrections, if applied, would move the curve about 0.05 mag to the right, slightly improving the match. The fit is quite good, although the bluest, hottest stars tend to be a little hotter than the models predict, as discussed above. The log g plot shows a mean around log g=8.1 (8.06 for the DAs and 8.22 for the DBs as determined from our tables), slightly higher than results from Bergeron et al. (1992a), for example, at log g=7.909. We also see a significant rise in log g for the redder objects, starting around $(u-i)_\circ = 0$, corresponding to a temperature around 12,000K. Figure 10 plots the histogram (and median) of the log g and $T_{\rm eff}$ fits for our DA and DB spectra with $S/N \geq 10.0$. This Figure includes our fits to all stars except those with *CH:* and clearly shows the bi-modal log g distribution seen in Figure 9. The excess at log g=9.0 in these plots is an artifact of our model grid which has an upper log g limit of 9.0.

Bergeron et al. (1990) found that the mean gravity and mass of a sample of DA white dwarf stars cooler than the ZZ Ceti instability strip was higher than for samples of hotter DA stars (cf. $T_{\rm eff} > 15,000K$, Bergeron, Saffer & Liebert, 1992a). The parameter fits for white dwarf stars cooler than 15,000K depend on the parameterization of convection (Bergeron, Wesemael, & Fontaine, 1992b) down to very cool temperatures where the convective temperature gradient becomes adiabatic. One interpretation of what appeared to be a systematic offset to higher log g of the cool white dwarf stars in the Bergeron analyses was that the mean mass was the same, but moderate amounts of helium have been convectively mixed into the atmosphere (Bergeron et al. 1990). Introducing helium and increasing the gravity affect Balmer line profiles in the same way by increasing atmospheric pressures and densities. Alternatively, one might expect the coolest (and oldest) white dwarf stars to have a higher than average mean mass since their mean progenitor mass may also be higher. This possibility is evaluated for the cool white dwarf sample by Bergeron, Leggett, & Ruiz (2001) who only show marginal evidence for such a mass increase with decreasing temperature. Besides, the higher mean gravity seen here seems to begin at about 11,000K where the cooling age is only about 1 Gyr. A third possibility for explaining the higher apparent masses and gravities of cool DA stars is that there is a systematic error in the models — perhaps a problem with the physics of the hydrogen level occupation probability (Hummer & Mihalas 1988), or in the parameterization of convection.

Figure 11 shows the object subclass classifications as a function of $(u-i)_\circ$. The six panels show the $(u-i)_\circ$ histogram for the human classified DAs, DBs, DOs, DCs, DQs, and DZs, respectively. All subtypes within each major classification and all solidly-identified spectra (regardless of S/N) are included. It is reassuring to see the DCs start at $(u-i)_\circ$ values where the DBs stop, the objects now being too cool to show He I lines. The DOs also end where the DBs start for similar reasons. The DQ stars, however, do overlap the DB region and are discussed further in Liebert et al. (2003a).

Figure 12 is a reduced proper motion plot of our white dwarf sample with proper motions greater than 12 mas yr^{-1}. The reduced proper motion, H_g, is calculated from $g+5\times\log\mu+5$ and is meant to approximate an absolute g magnitude by using the measured proper motion as a proxy for distance. We plotted the white dwarf binaries (the WD+M objects) with a different symbol since their colors will be skewed by the binary companion. The curves show Bergeron, Wesemael, & Beauchamp (1995) DA models (convolved through SDSS filters) with assumed tangential velocities of 10 and 300 km s^{-1}. As expected, the observed white dwarf population falls nicely between these two extremes.

7. Some Interesting Objects

Undoubtedly in a catalog that nearly doubles the number of previously known white dwarf stars, there are going to be some interesting, peculiar objects contained within. Harris et al. (2003) already discuss several such objects and we point out a few more here.

7.1. Low-mass DAs

Traditionally, astronomers have followed Greenstein & Sargent (1974) in defining a star with $\log g \geq 7.0$ as a white dwarf, and lower gravity objects, subdwarf or main sequence stars. Existing white dwarf samples appear to include a component of low mass stars (< 0.5 solar), with cores composed of helium rather than carbon-oxygen. These may be identified from low surface gravity fits, or from inference based on a trigonometric parallax and luminosity determination. Many of these candidates have been shown to be binaries, the companion being either another white dwarf (eg. Marsh, Dhillon & Duck 1995) or a low mass main sequence star (Zuckerman & Becklin 1992).

A number of stars in this catalog fit $\log g < 7.5$, which suggests a mass near or below 0.45 solar unless the temperature is above 40,000K. Low mass white dwarf stars have much larger radii at high temperatures than at lower temperatures. Four very low mass candidates with $\log g < 7.0$ include (1) SDSS J002207.65–101423.5 with $T_{\rm eff} = 19672$ and $\log g = 6.82$, (2) SDSS J234536.48–010204.8 at 33049K and 6.74, (3) SDSS J105611.03+653631.5 at 20290, 6.97, and (4) SDSS J142601.48+010000.2 at 16465, 6.97. Unfortunately, the signal-to-noise ratio of the spectra allow low but less extreme gravities in all cases, and reobservation of these stars is desirable if the goal is to identify white dwarf stars of very low mass.

One object, SDSS J123410.37–022802.9, has a spectrum good enough in quality that there is no doubt about its low mass. Our fit which measured $T_{\rm eff} = 17308$K and $\log g = 6.34$ is shown in Figure 13. We will defer discussion of this so-far unique object to a separate paper (Liebert et al. 2004).

The DAs which we fit with $\log g$ values between 6.7 and 7.0, all with significant proper motions, are listed in Table 9.

7.2. High-mass DAs

More than 20 DA stars shown in Figure 9 have a fit indicating high gravity, implying a mass significantly higher than the average mass for white dwarf stars. Examination of their spectra indicates the fits are generally good and the gravity determinations are probably correct in most cases. Many of the stars are faint, however, and followup spectra are desirable. Some of these stars have two other features that provide support for the high gravity results: first, their *ugr* colors (Figure 1) often lie above and to the left of the main DA sequence as a result of their high gravities; second, their reduced proper motions (Figure 12) are often large, consistent with a low luminosity (hence closer distance) caused by a high mass and small radius. Occasional photometric errors or incorrect dereddening, and the statistical nature of reduced proper motions (strongly affected by occasional stars with high space velocities), mean that neither of these features give a definitive confirmation of the high gravities, only indicative support. Table 10 lists our best candidates for massive DAs with $\log g > 8.5$.

7.3. Ultra-cool White Dwarf Stars

Harris et al. (2001) discuss the two ultra-cool white dwarf stars found by the SDSS. One, SDSS J133739.40+000142.9, is a unique discovery of the SDSS while the second, SDSS J165401.26+625355.0, was previously known as LHS 3250 and is discussed in Harris et al. (1999). Both are believed to have low masses and helium cores. LHS 3250 has a measured parallax, and Bergeron & Leggett (2002) find that including the parallax gives a solution with $\log g = 7.27$ and a mass of 0.23 $M_{\odot}$. We found no more similar objects in the expanded DR1 data set.

It thus appears that the LHS 3250-like white dwarf stars, with very strong opacity due to collisionally-induced absorption (CIA) bands of molecular hydrogen, are quite rare. Bergeron & Leggett (2002) showed quantitatively that LHS 3250 is a very low mass helium object. In the discovery paper, Harris et al. (2001) pointed out that it is kinematically a likely member of the disk, not the halo population. Indeed, Althaus et al. (2001) and Serenelli et al. (2001) demonstrate that low mass helium core white dwarf stars (with hydrogen envelopes) evolve into the regime where the CIA opacity becomes dominant in the infrared to I band in a shorter time than do white dwarf stars of normal mass (ie. arguably, within the age of the disk, not the halo). The SDSS sample has uncovered no candidates of more normal mass from the Galactic halo.

One caveat has to be added, however. The very cool candidate WD 0346+246 discussed by Hodgkin et al. (2000) *does* have halo kinematics, but it may not show the CIA opacity strongly enough to be pulled out of the stellar locus were it observed by the SDSS — which is how LHS 3250 and SDSS 1337 were found. Hence, the conclusion of the previous paragraph does not rule out the presence of many cool, halo white dwarf stars in the SDSS imaging data.

7.4. Hot DBs?

There are 12 DBs in Table 4 that fit to a $T_{\rm eff} > 30,000K$. Since no DB has yet to be found above 30,000K, the so-called "DB gap" (Liebert 1986), these are very interesting objects!

Two of these objects, SDSS J163838.24–005417.5 and SDSS J040854.60–043354.7 show obvious signs of hydrogen in their spectra while SDSS J090456.13+525029.9 shows perhaps a weak hint of Hα. The fit to SDSS J102615.54+005942.9 has two minima and the spectrum is quite noisy (as indicated by the large uncertainty in the $T_{\rm eff}$ determination), so it may just be that the proper fit is the cooler, second minimum. In addition, SDSS J203517.50-064539.9's fit includes a *:* which arose from a bad match between the fit spectrum and the SDSS photometry.

The remaining seven objects, however, seem to have acceptable fits, no visible sign of hydrogen in their spectra and colors which generally agree with a $T_{\rm eff}$ at or above 30,000K. Given the systematic uncertainties in our model fitting, as well as the noise in these spectra, we do not claim these objects as certain occupants of the DB gap. Better spectra and more careful fitting will be required to assess these remaining, potentially very intriguing hot DBs.

7.5. An Eclipsing, Pre-Cataclysmic Variable?

The DA SDSS J010622.99–001456.3 is another interesting case. Its *best* photometric magnitudes as listed in our tables indicate a very dim red object, (u,g,r,i,z)=(25.3, 24.8, 20.7, 20.8, 19.5), whereas the spectrum appears like a substantially brighter 11,000K DA. These u and g magnitudes are basically non-detections. The SDSS *best* image of the object looks fine except for the presence of a very dim, red object instead of the brighter, bluer one we would expect to see. The *target* photometry, (u,g,r,i,z)=(18.6, 18.1, 18.3, 18.5, 18.3), shows it to be a normal, bluish, bright DA, in good agreement with the spectrum. We actually have six separate imaging observations of this object and in all but one case (the one ironically labeled *best*), the magnitudes agree with both the *target* data and the spectrum.

The spectrum does show some possible (although noisy) excess in the red, perhaps indicating a faint red companion, which if it occasionally produces a total eclipse of the white dwarf star, could explain the one deviant set of photometric measurements. Our fit to the spectrum supports this idea; the white dwarf appears bluer than the model. The *best* $(r-i)$ and $(i-z)$ magnitudes are not quite right for a typical late-type star, but there is a time delay between each filter measurement, so we could be seeing some of the white dwarf in one filter and more or less in another, as the eclipse progresses.

The previously-known object PG1413+015 (GK Vir: Green et al. 1978, Fulbright et al. 1993, Green, Schmidt, & Liebert 1986) is an eclipsing binary system consisting of a DAO white dwarf star with a roughly M4 V companion. Its orbital period is $8^{\rm h}16^{\rm m}$ which places it among the shortest period white dwarf binaries that do not show signs of interaction with its companion. The natural evolution of this system is thought to lead to a cataclysmic variable and thus it represents a rare pre-cataclysmic system. Whether or not SDSS J010622.99–001456.3 is a similar system will require future observations, but current observations are consistent with such an interpretation. We are now planning to observe this star periodically for radial velocity and color changes.

7.6. One Non-Cataclysmic-Variable

The star SDSS J131751.72+673159.4 is classified here as DAME, showing sharp H and HeI emission lines in the cores of the broader absorption lines of the white dwarf. The emission lines are sharper than those seen in the numerous SDSS spectra of cataclysmic variables (CVs) (Szkody et al. 2002, 2003). This star must have a close cool companion, and may become a CV, but it is not a CV now. It is listed in the online version of the Downes et al. (2001) CV Catalog, where we suggest it should be deleted.

7.7. DAs with Weak Balmer Lines

Three interesting stars are classified as DA: in Table 6: SDSS J102448.85-002312.3, SDSS J150856.89+013557.8, and SDSS J164306.06+442638.1. They all have significant proper motions, colors indicating temperatures between about 10000–14000 K, and weak Hα and possibly higher Balmer lines. If they were normal DA white dwarf stars, they would have much stronger Balmer lines. They are likely to be white dwarf stars with atmospheres dominated by helium but including a small amount of hydrogen. They would appear as DBA stars if they were a little hotter, or DC stars if they were cooler.

8. Conclusions

By selecting candidate spectra based mostly on a variety of color and proper motion cuts, we have found 2791 spectroscopically-confirmed white dwarf and subdwarf stars in the first data release of the SDSS. We currently see no reason why this detection rate should change in future SDSS data releases, and thus can look forward to an additional 10,000 or so white dwarf stars from the SDSS by the time it is finished.

This and future catalogs will allow us to expand dramatically our sample of particularly unique, interesting, and rate white dwarf stars. We have already pointed out some of the work going on in this regard with the DQ, DH, pulsating, and hot DO white dwarf stars.

We expect to make updated catalogs available as more data are released by the SDSS and welcome contact with fellow white dwarf researchers with regards to SDSS objects.

An ultimate goal of white dwarf research is a vastly improved luminosity function over what is known at present. The vagaries of how SDSS white dwarf spectra are obtained makes building a full luminosity function a difficult task, but one which should be ultimately possible. However, a luminosity function concentrating on the hot end of the white dwarf cooling sequence suffers from fewer targeting complications and thus should be doable on much shorter timescales than the entire luminosity function will require. We are currently beginning this work in addition to preparing the next public catalog of white dwarf stars from the SDSS. The data tables presented here are available online at the SDSS DR1 value added catalog site: http:///www.sdss.org/dr1/products/value_added/wdcat/dr1/index.html.

We are grateful to Detlev Koester for providing us his fine grid of DA and DB models we used in our model fits. SJK, AN, and JK would like to thank J. Peoples and B. Gillespie for their support of our research effort. D.J.E. was supported by NSF AST-0098577 and an Alfred P. Sloan Research Fellowship.

Funding for the creation and distribution of the SDSS Archive has been provided by the Alfred P. Sloan Foundation, the Participating Institutions, the National Aeronautics and Space Administration, the National Science Foundation, the U.S. Department of Energy, the Japanese Monbukagakusho, and the Max Planck Society. The SDSS Web site is http://www.sdss.org/.

The SDSS is managed by the Astrophysical Research Consortium (ARC) for the Participating Institutions. The Participating Institutions are The University of Chicago, Fermilab, the Institute for Advanced Study, the Japan Participation Group, The Johns Hopkins University, Los Alamos National Laboratory, the Max-Planck-Institute for Astronomy (MPIA), the Max-Planck-Institute for Astrophysics (MPA), New Mexico State University, University of Pittsburgh, Princeton University, the United States Naval Observatory, and the University of Washington.

A. Comparison with the McCook and Sion White Dwarf Catalog

Matching the stars in this paper with those in the online version of the McCook & Sion (1999) catalog combined with a preliminary list of WDs found in the Hamburg Quasar Survey (Homeier et al. 1998) finds 109 white dwarf stars (one of which we find to be a sdB star) in this paper have been already published, not counting those SDSS WDs already reported by Harris et al. (2003) and Raymond et al. (2003). These previously known stars are listed in Table 11. Not surprisingly, these stars tend to be relatively bright and our spectral classifications are generally consistent with those published previously. Different SDSS positions compared to the previously published positions noted for some stars in the table can usually be understood by the stars' proper motions and/or by truncation or imprecise original coordinates — the SDSS coordinates should be used.

We also searched the McCook and Sion (1999) catalog for white dwarf stars that fell within the 2099 $\deg^2$ of the DR1 imaging sky area, but which were not recovered by us. Remember, the SDSS targeting of white dwarf stars for spectroscopy is rather haphazard; most of our spectra come from targeting categories other than those searching for white dwarf stars and are thus "rejects" of these other categories. However, we find only 218 known white dwarf stars within the DR1 imaging area for which we do not have spectra. This number includes objects in the 769 $\deg^2$ of DR1 imaging area that do not currently have DR1 spectra. Some of these objects may still get SDSS spectra that will become available in a future data release. uture objects, along with the SDSS PSF magnitudes and errors, are shown in Table 12. The coordinates listed are those from the SDSS. Since many known white dwarf stars are too bright for the SDSS to measure accurately, any magnitude which is flagged as *SATURATED* in the DR1 database is marked with an * next to the listed magnitude. SDSS saturated magnitudes are not reliable.

REFERENCES

Abazajian, K., et al., 2003, AJ, 126, 2081

Althaus, L.G., Serenelli, A.M., Benvenuto, O.G. 2001, MNRAS, 323, 471

Anderson, Scott F., et al., 2003, AJ, in press, astro-ph/0305093

Becker, R.H., White, R.L., & Helfand, D.J., 1995, ApJ, 450 559

Bergeron, P., Wesemael, F., Fontaine, G., and Liebert, James, 1990, ApJ, 351, L21

Bergeron, P., Saffer, Rex A., & Liebert, James, 1992, ApJ, 394 228

Bergeron, P., Wesemael, F., & Fontaine, G., 1992, ApJ, 387, 288

Bergeron, P., et al., 1994, ApJ, 432, 305

Bergeron, P., Wesemael, F. & Beauchamp, A., 1995, PASP, 107, 1047

Bergeron, P., Leggett, S.K., & Ruiz, M.T., 2001, ApJS, 133, 413

Bergeron, P. & Leggett, S.K., 2002, ApJ, 580, 1070

Blanton, M., et al., 2003, AJ, 125, 2276

Boyle, B.J., et al., 2000, MNRAS, 317 1014

Cardelli, J.A., Clayton, G.C., & Mathis, J.S., 1989, ApJ, 345, 245

Downes, R.A., Webink, R.F., Shara, M.M., Ritter, H., Kolb, U., & Düerbeck, H.W. 2001, PASP, 113, 764

Fan, X., 1999, AJ, 117, 2528

Finley, David S., Koester, Detlev, & Basri, Gibor, 1997, ApJ, 488, 375

Fukugita, M., Ichikawa, T., Gunn, J. E., Doi, M., Shimasaku, K., Schneider, D. P., 1996, AJ, 111, 1748

Fulbright, Michael S., Liebert, James, Bergeron, P., & Green, Richard, 1993, ApJ, 406, 240

A&A, 394, 957

Green, R.F., Richstone, D.O., & Schmidt, M. 1978, ApJ, 224, 892

Green, Richard F., Schmidt, Marten, & Liebert, James, 1986, ApJS, 61, 305

Gunn, J.E., et al., 1998, AJ, 116, 3040

Greenstein, Jesse L. & Sargent, Annelia, I., 1974, ApJS, 28, 157

Harris, H., et al., 1999, ApJ, 524, 1000

Harris, H., et al., 2001, ApJ, 549, 109

Harris, H., et al., 2003, AJ, in press

Hodgkin, S., et al. 2000, Nature, 403, 57

Hogg, D.W., Finkbeiner, D.P., Schlegel, D.J., & Gunn, J.E. 2001, AJ, 122, 2129

Homeier, D., et al., 1998, A&A, 338, 563

Hummer, D.G. & Mihalas, D. 19,88, ApJ,, 331, 794

Koester, D., et al., 2001, A&A, 378, 556

Krzesinski, Jurek, et al., 2004, submitted to A&A

Liebert, James, 1986, ASSL Vol. 128: IAU Colloq. 87: Hydrogen Deficient Stars and Related Objects, 367

Liebert, James, et al., 2003, AJ, 126, 2521

Liebert, James, et al., 2004, in preparation

Marsh, T.R., Dhillon, V.S., & Duck, S.R., 1995, MNRAS, 275, 828

Marsh, M.C., et al., 1997, MNRAS, 386, 369

McCook, George P. & Sion, Edward M., 1999, ApJS, 121, 1

Monet, D.G., et al., 2003, AJ125, 984

Mukadam, Anjum, et al., 2004, submitted to ApJ

Munn, J., et al., 2003, in preparation

Napiwotzki, R., Green, P.J., & Saffer, R.A., 1999, ApJ, 517, 399

Nitta, A., et al., 2004, in preparation

Pier, J.R., et al., 2003, AJ, 125, 1559

Raymond, Sean, N., et al., 2003, AJ, 125, 262

Richards, Gordon T., 2002, AJ, 123, 2945

Schlegel, D.J., Finkbeiner, D.P., & Davis. M., 1998 ApJ, 500, 525

Schmidt, G.D., et al., 2003, ApJ, 595, 1101

Serenelli, A.M., Althaus, L.G., Rohrmann, R.D., & Benvenuto, O.G. 2001, MNRAS, 325, 607

Sion, Edward M., Greenstein, Jesse L., Landstreet, John D., Liebert, James, Shipman, Harry L., & Wegner, Gary A., 1983, ApJ, 269 253

Smith, J. Allyn, et al., 2002, AJ, 123, 2121

Stoughton, C., et al., 2002, AJ, 123, 485

Skzody, P., et al., 2002, AJ, 123, 430

Szkody, P., et al., 2003, AJ, 126, in press

Tremonti, C., et al., 2003, in preparation

Vennes, S., Thejll, P., Galvan, R.G., & Dupuis, J., ApJ, 480, 714

Vennes, S., et al., 2002, MNRAS, 335, 673

Voges, w., et al., 1999, A&A, 349, 389

York, D.G., et al., 2000, AJ, 120, 1579

Zuckerman, B., & Becklin, E.E., 1992, ApJ, 386, 260

This preprint was prepared with the AAS LaTeX macros v5.0.

Fig. 1.— $(u-g)_\circ$ vs. $(g-r)_\circ$ color-color diagram for the many types of white dwarf stars identified here. The WDM classification refers to white dwarf stars with any non-degenerate companions, virtually always an M or sdM dwarf star.

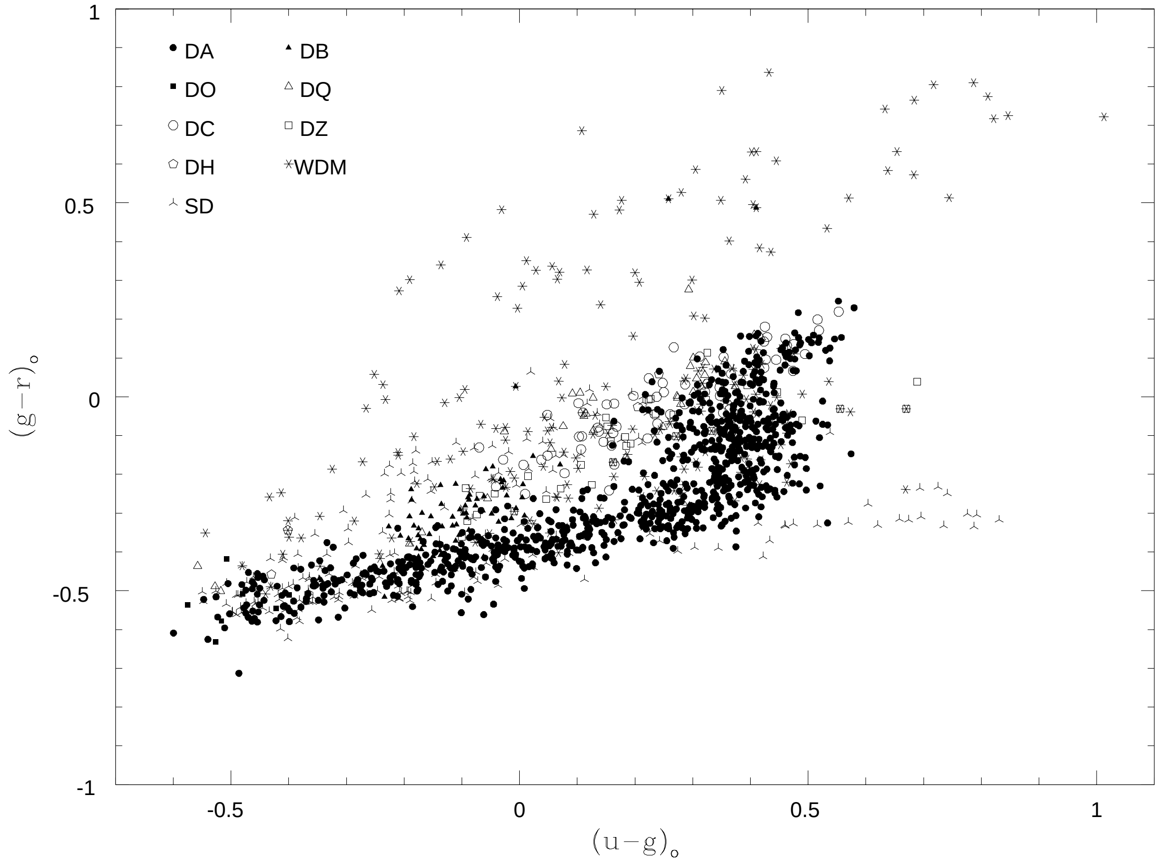

Fig. 2.— $(g-r)_\circ$ vs. $(r-i)_\circ$ color-color diagram for the many types of white dwarf stars identified here. The WDM classification refers to white dwarf stars with any non-degenerate companions, virtually always an M or sdM dwarf star.

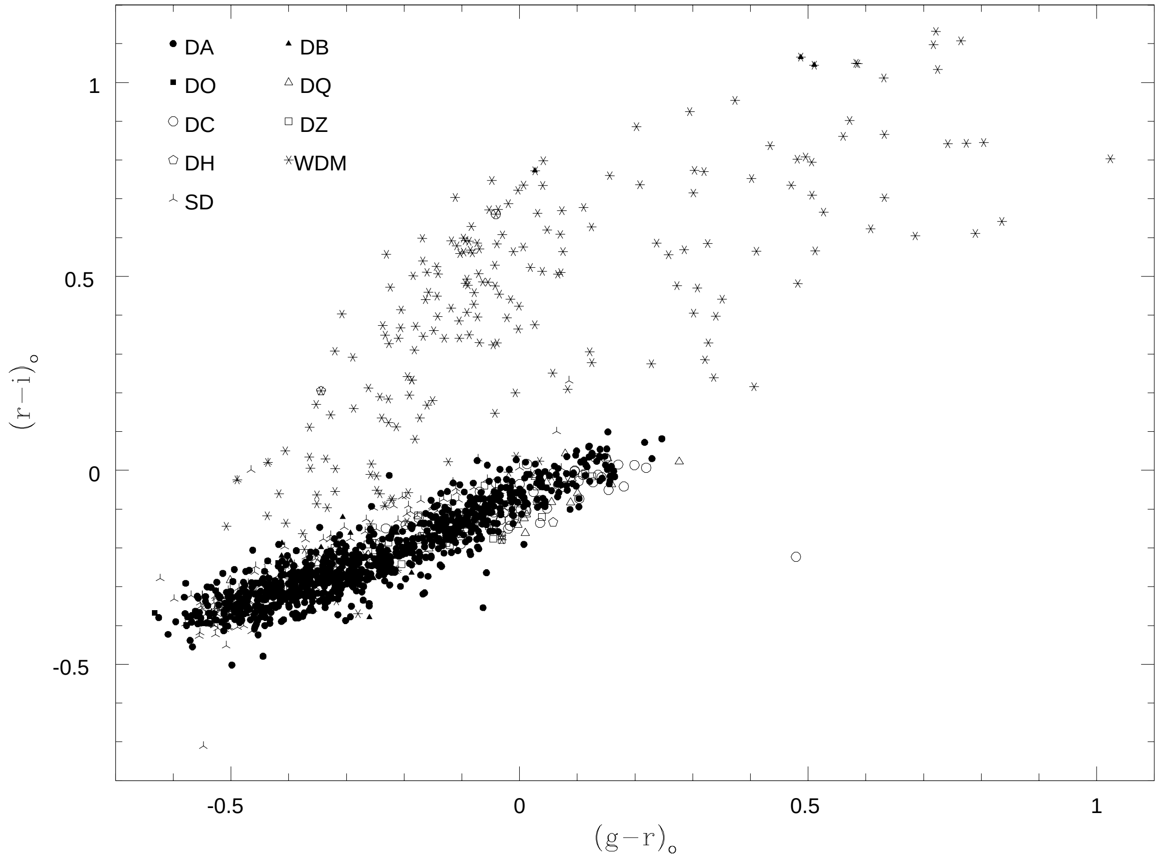

Fig. 3.— Our model fit to the $g = 16.9$ DA, SDSS J074041.67+412107.4.

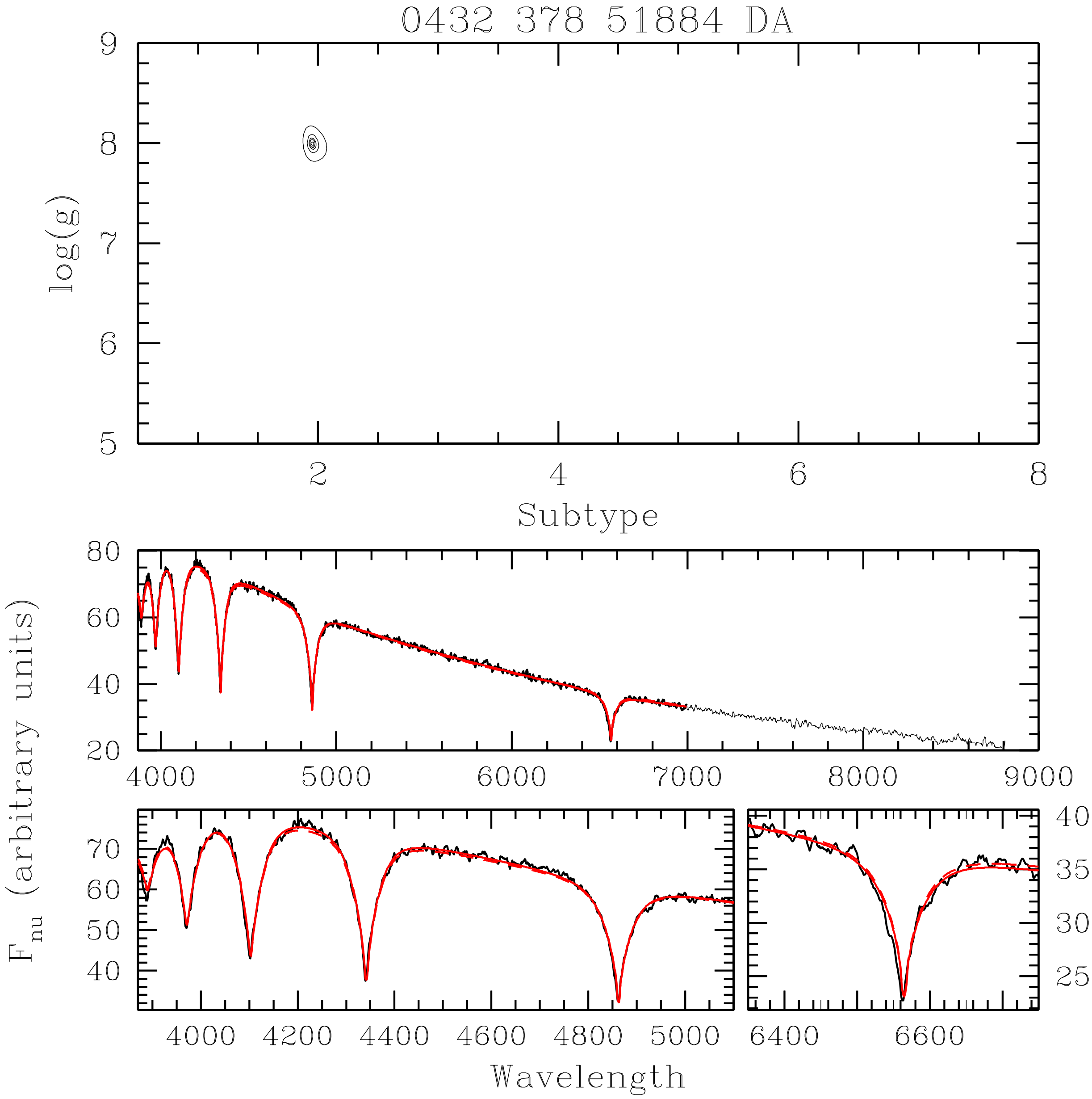

Fig. 4.— Our model fit to the $g = 20.5$ DA, SDSS J073651.84+375545.1.

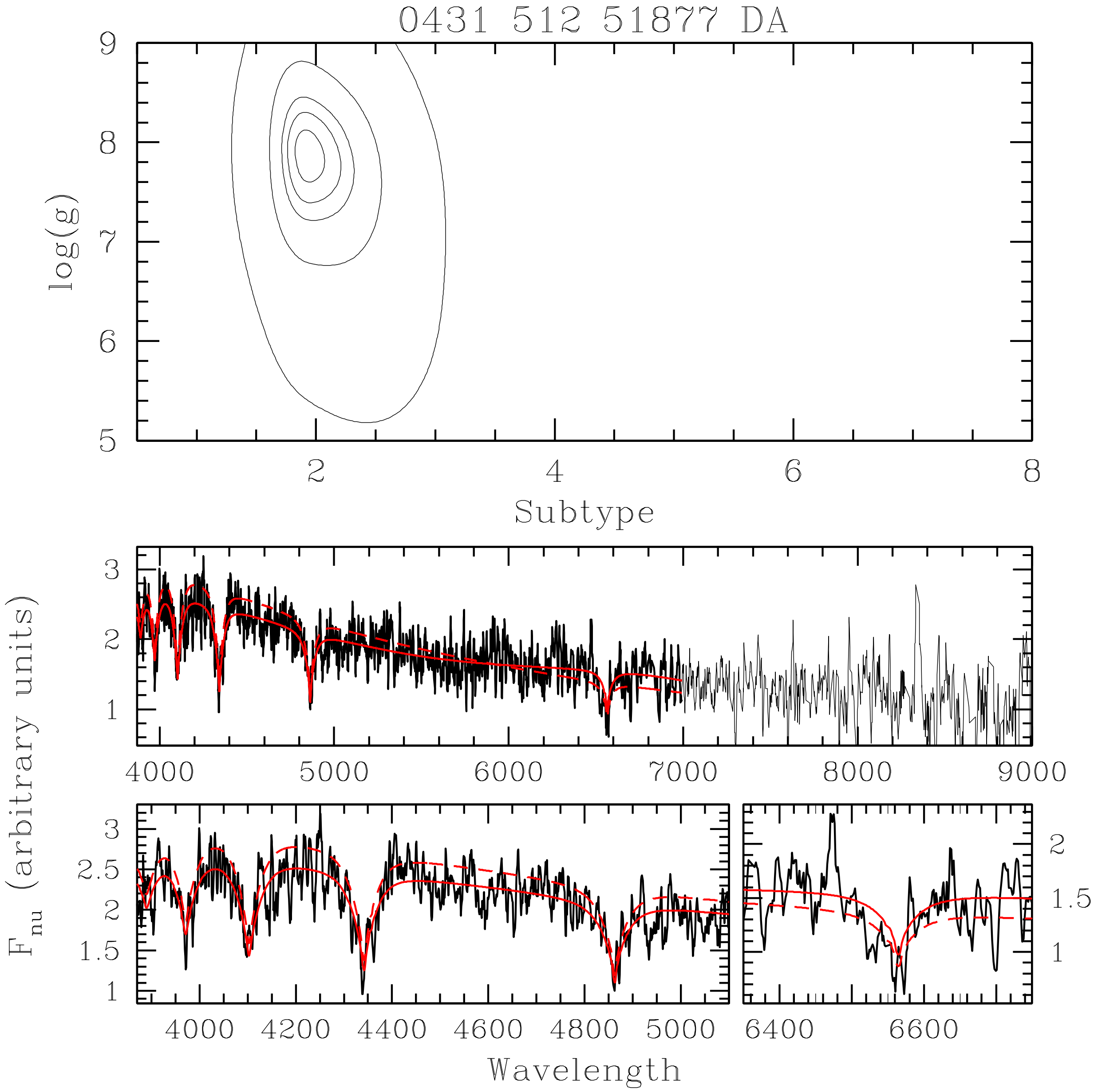

Fig. 5.— Our model fit to the $g = 18.9$ DB, SDSS 002633.89+005425.9.

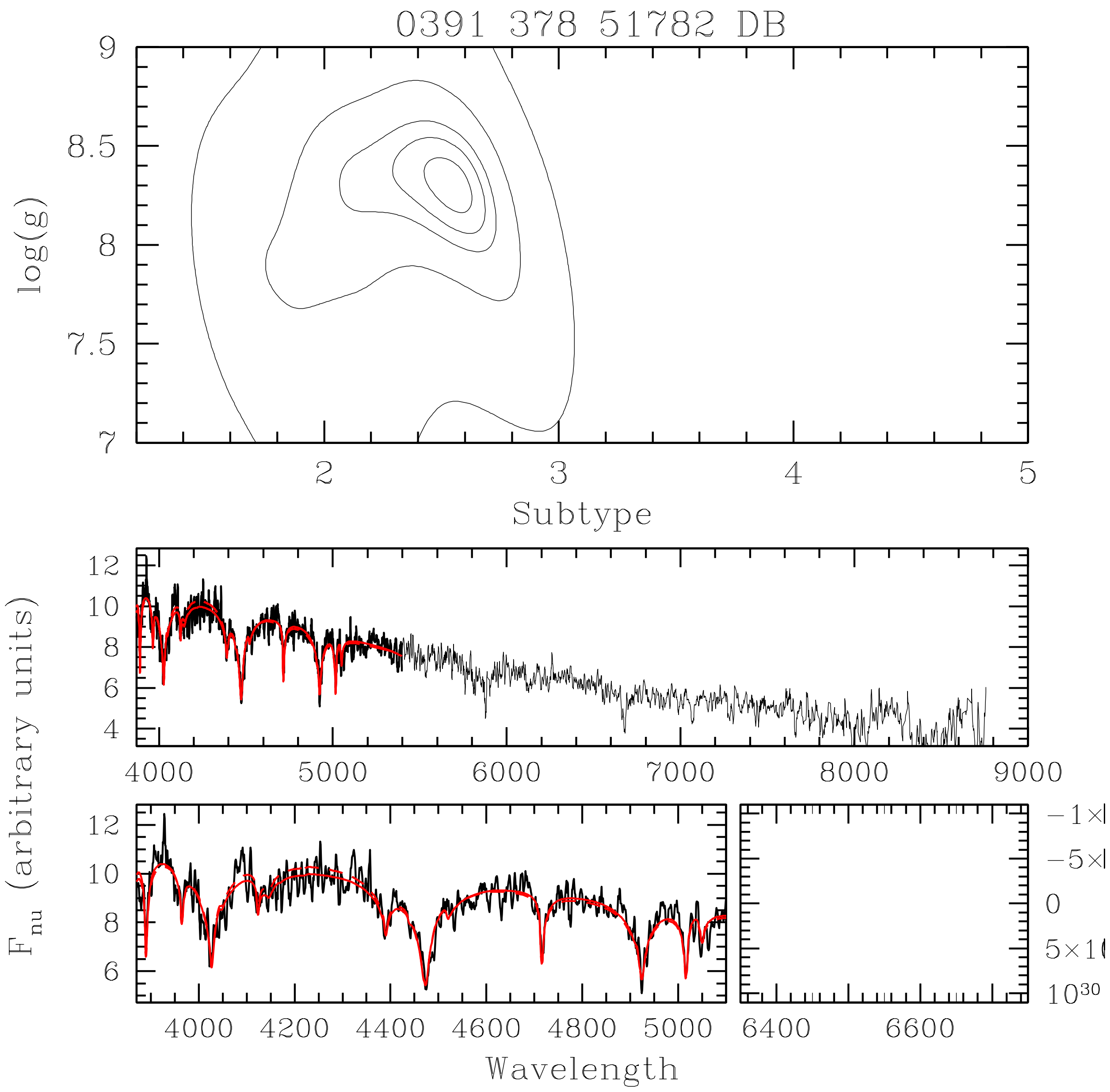

Fig. 6.— The distribution of errors in our fits of repeat spectra for DAs (left) and DBs (right). The y-axis is the difference in the T_{eff} determinations from each fit divided by the sum in quadrature of the two T_{eff} uncertainties. The x-axis is the similar quantity for log g. The ellipses are the contours that should include 68%, 95%, and 99.7% of the points if the distributions were Gaussian (and independent).

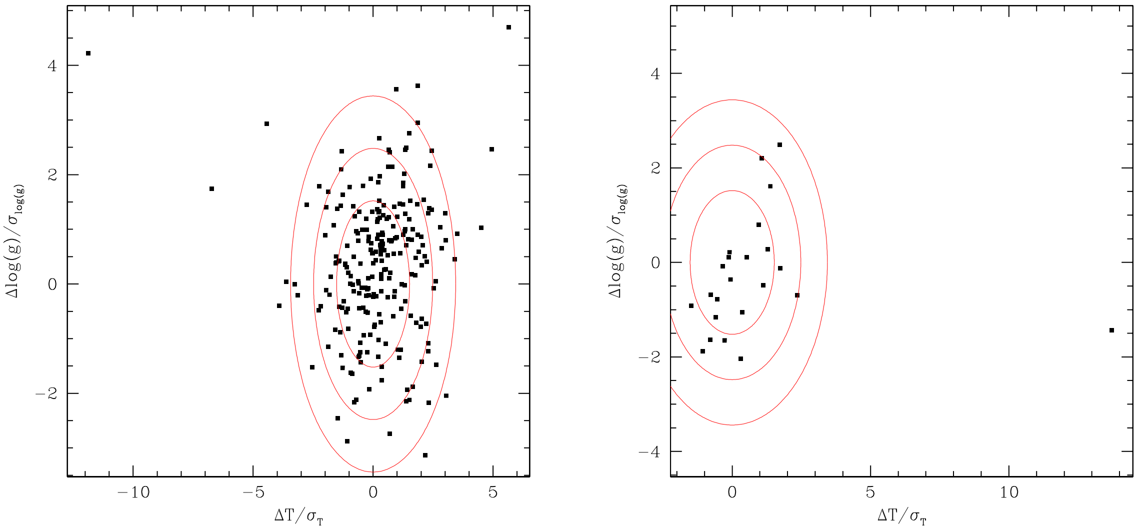

Fig. 7.— Relative temperature (left) and absolute log g (right) differences between our (autofit) fits and literature (lit) fits for already known DA stars. The squares are based on published fits based on Koester models, the circles are based on Bergeron models, and the asterisks are based on other models.

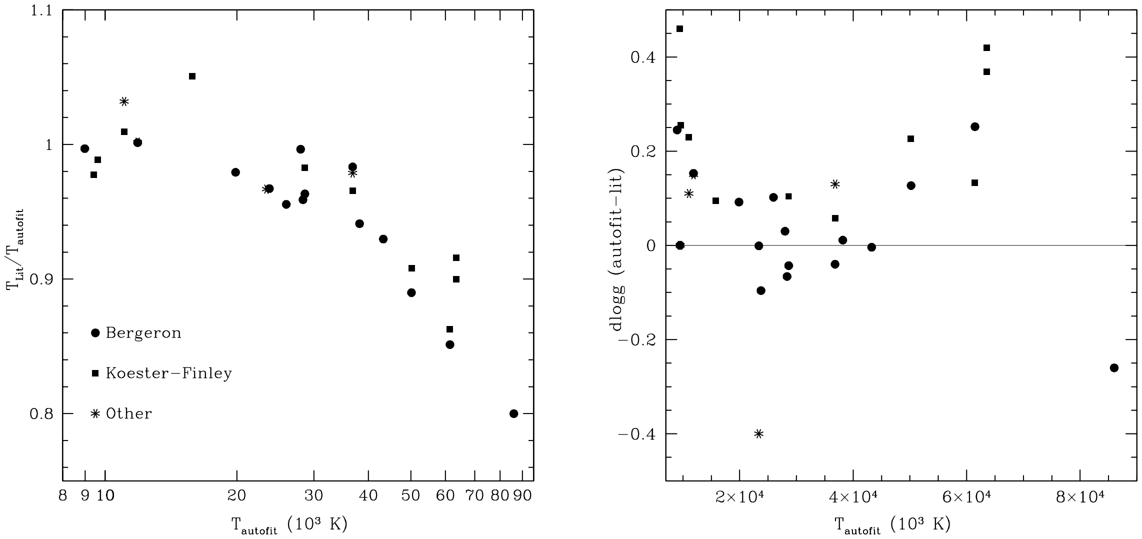

Fig. 8.— T_{eff} vs. $(u-i)_\circ$ from our DA and DB model fits. We include only data with the spectroscopic S/N in $g>$ 10/pixel. The solid line represents Bergeron et al. (1995) models convolved with SDSS filter curves.

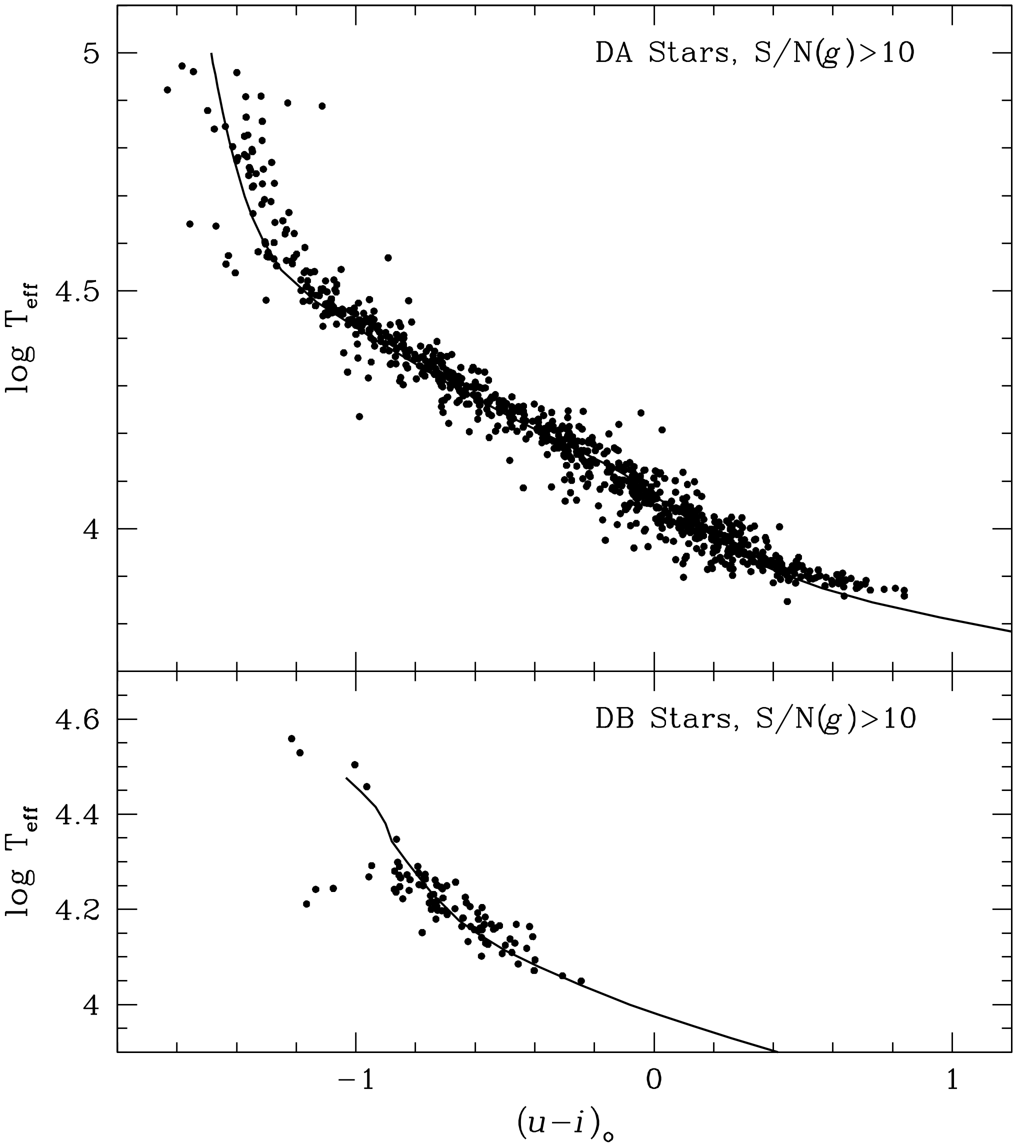

Fig. 9.— log g vs. $(u-i)_\circ$ from our DA and DB model fits. We include only data with the spectroscopic S/N in g> 10/pixel.

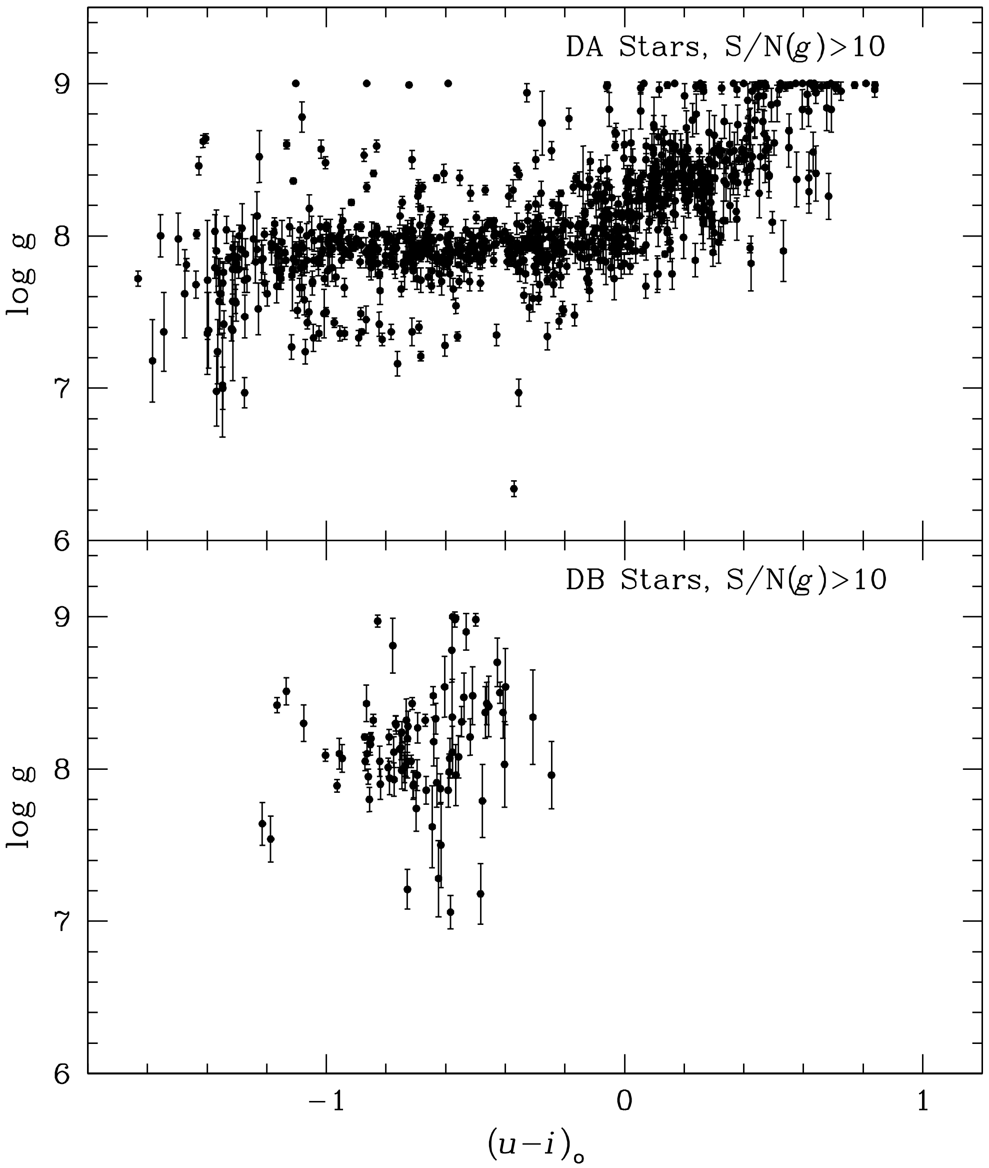

Fig. 10.— Histograms of DA and DB log g and T_{eff} fit values. We strongly suspect that our fits to high temperature DBs are inaccurate and thus the few DBs with fit temperatures greater than 30,000K are probably not so hot.

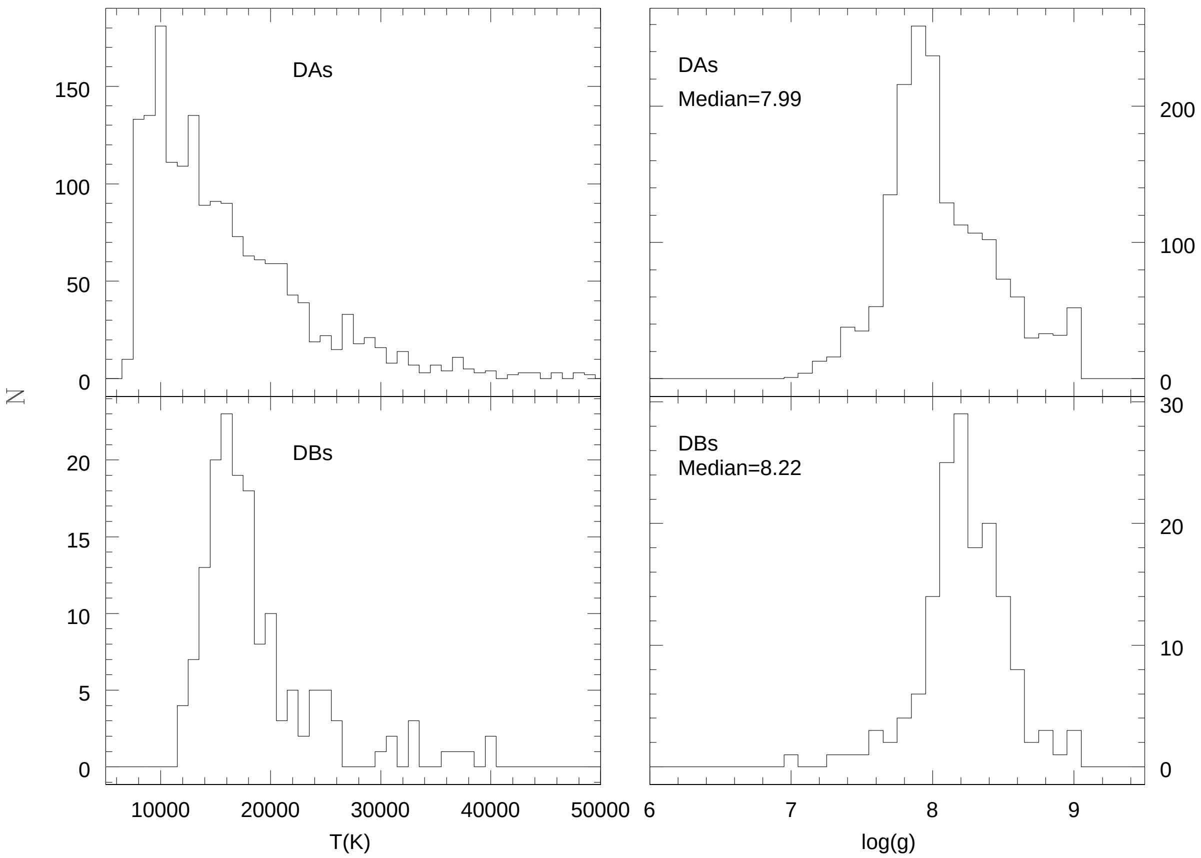

Fig. 11.— Histogram of white dwarf subclasses as a function of $(u - i)_{\circ}$.

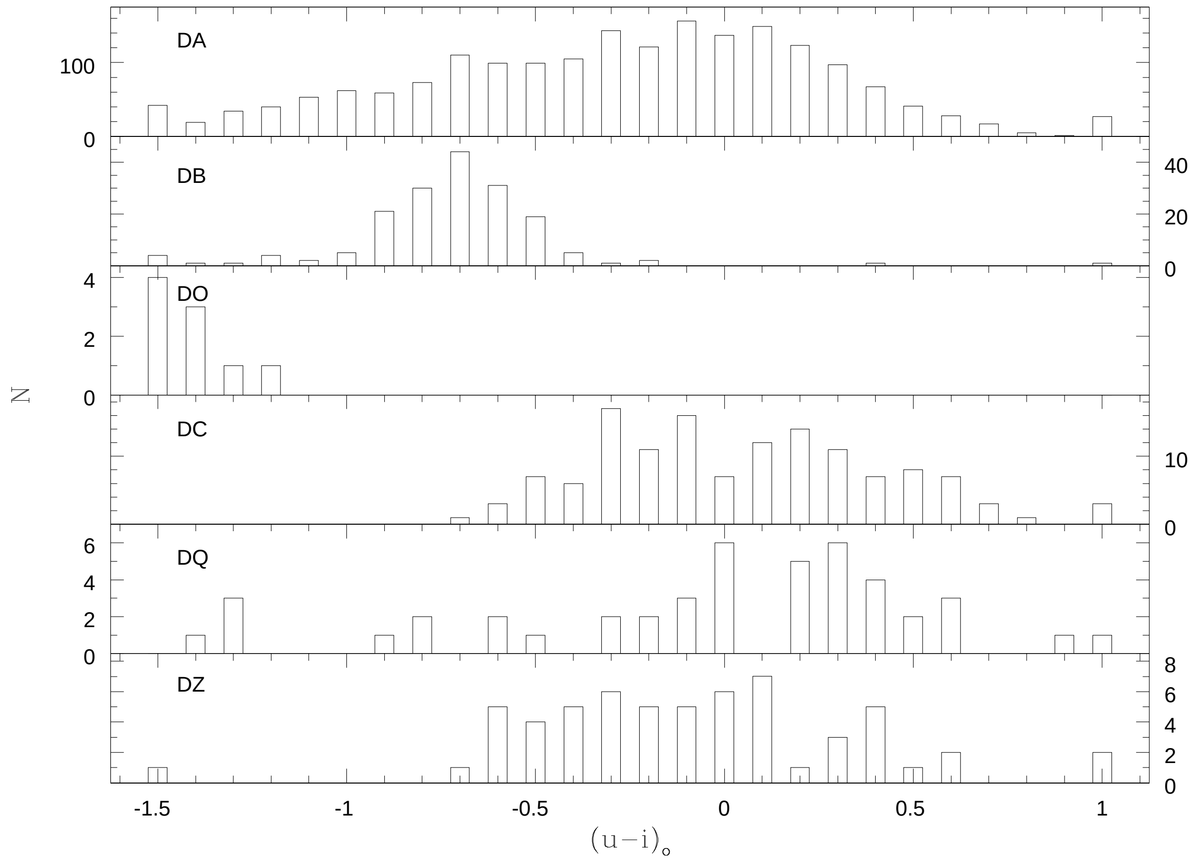

Fig. 12.— Reduced proper motion diagram of the white dwarf sample with proper motions > 12 mas yr^{-1}. The two curves are Bergeron et al. (1995) DA models convolved with SDSS filters with assumed tangential velocities of 10 and 300 km s^{-1}. The observed population of single white dwarf stars are contained quite well by these two curves.

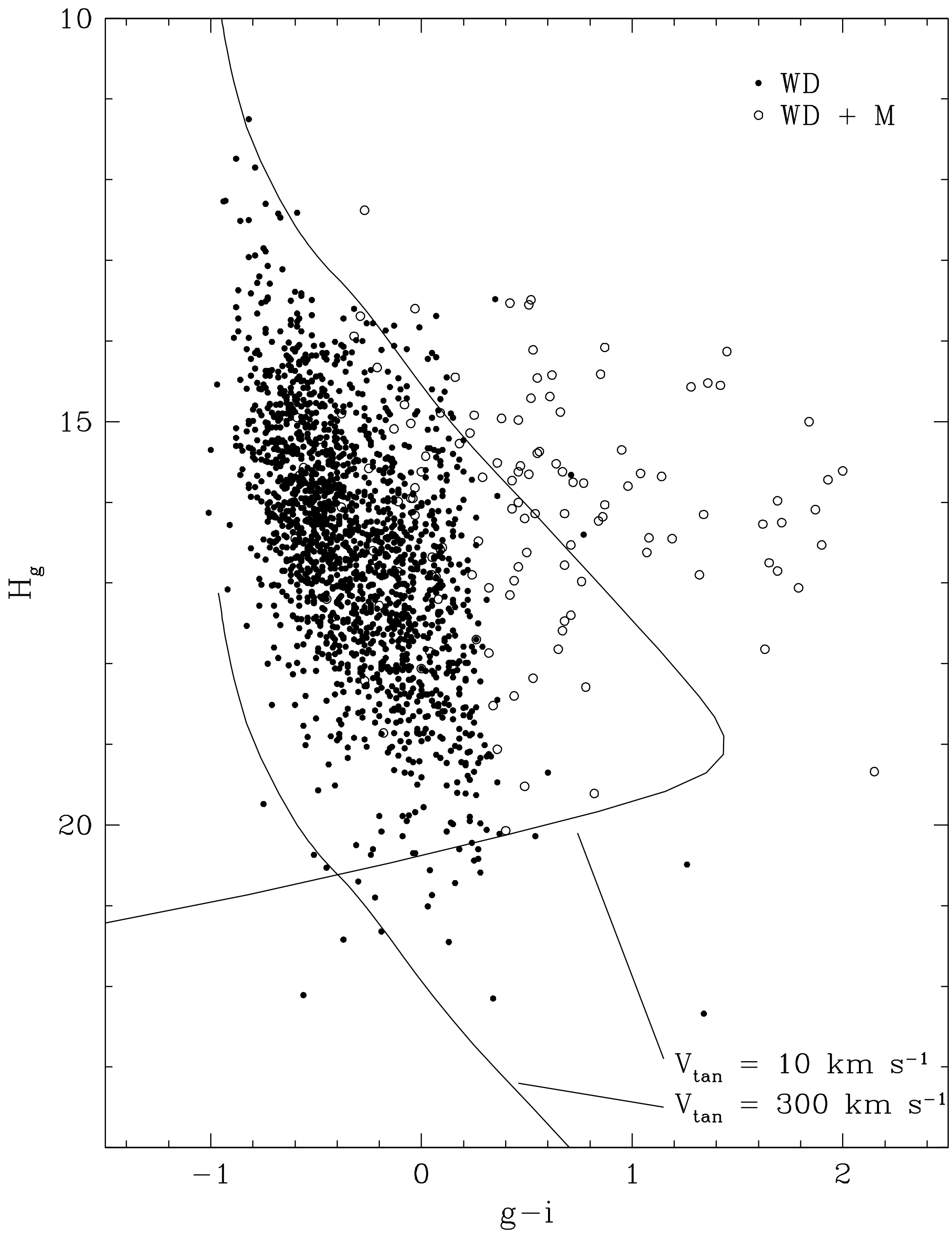

Fig. 13.— Our model fit to SDSS J123410.37-022802.9, a probable low mass DA.

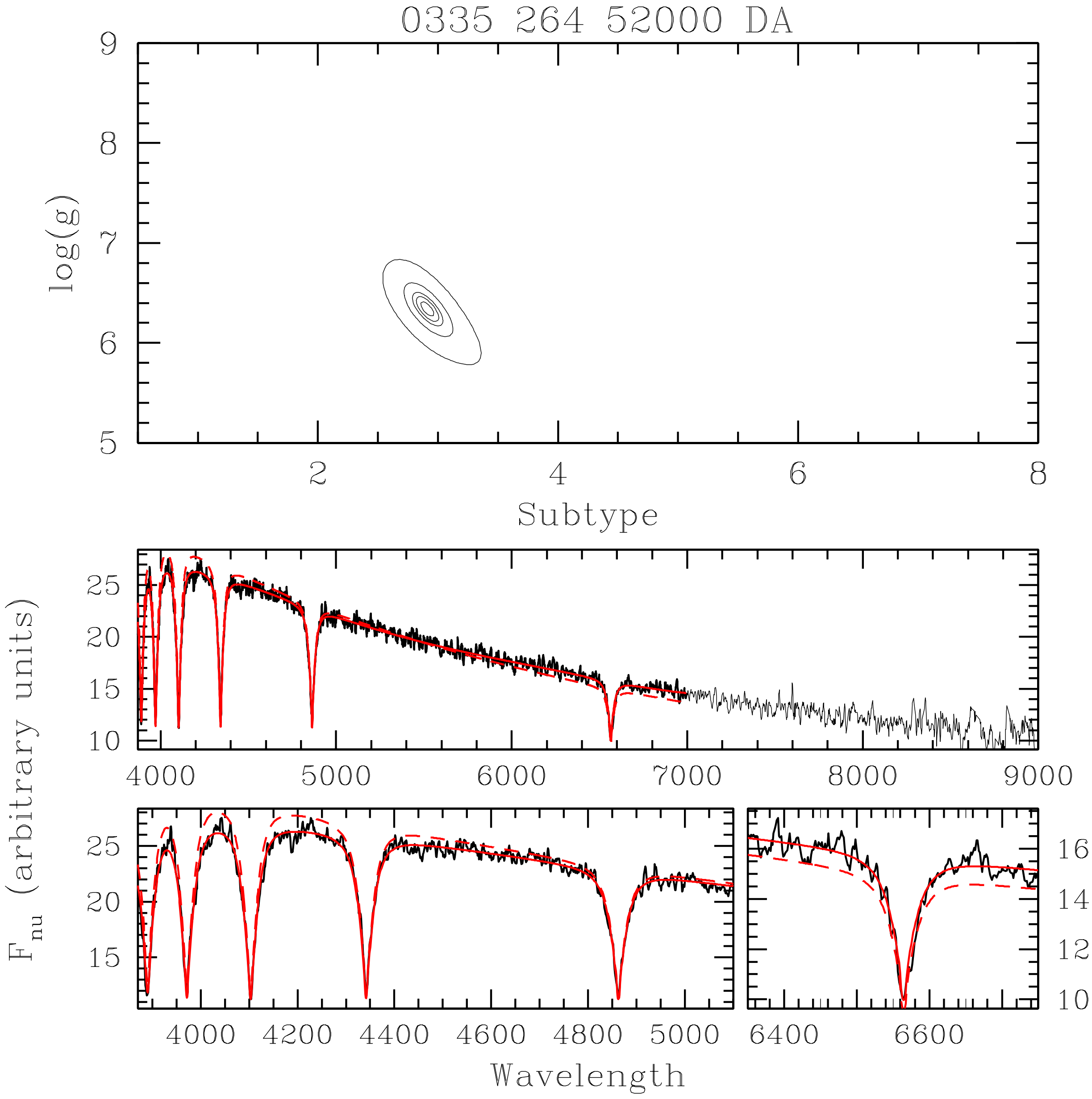

Table 1. SDSS targeting categories for all presented white dwarf and hot subdwarf spectra.

OBJTYPE	DAs	DBs	DOs	DCs	DQs	DZs	DHs	WDM	SDs	ALL
SERENDIPITY_MANUAL	3	0	0	0	0	0	0	1	0	4
GALAXY	0	0	0	0	0	0	0	3	2	5
ROSAT	9	1	0	0	0	0	0	0	0	10
QA	8	0	0	1	0	0	0	2	0	11
STAR_BHB	19	0	0	0	0	1	0	0	5	25
STAR_CATY_VAR	15	1	0	2	0	0	0	17	0	35
STAR_WHITE_DWARF	131	8	0	3	1	2	4	1	7	157
SERENDIPITY_DISTANT	417	34	0	6	2	6	4	1	34	505
HOT_STD	268	85	13	7	7	9	7	11	124	531
QSO	390	3	0	62	31	21	10	133	50	707
SERENDIPITY_BLUE	628	39	0	53	4	18	5	31	18	801

Note. — The numbers in the the individual category columns do not sum to those in the ALL column since the latter includes the certain white dwarf stars, but of uncertain subclass.

Table 2. Number of resultant objects, N, and criteria for candidate spectra selection.

Classification Type	Photometric Constraints	Other Constraints	N
Blue	$(u-g)_\circ < 0.70$ $(g-r)_\circ < -0.10$ $u < 21.0$	specClass != 3 (ie. object not a QSO)	4937
Medium Blue	$(u-g)_\circ < 0.60$ $(g-r)_\circ > -0.10$ $u < 21.0$	specClass = 0,1 or 6 (star or unknown) OR Zstatus = 0 or 1 or 2 (z measurement failed or inconsistent) OR z < 0.01	3553
Medium Red w/ Proper Motion	$(u-g)_\circ > 0.60$ $(g-r)_\circ < 1.00$ $H_g > 17.0$ [3] OR $H_g > 14.0 + 3.0 * (g-i)_\circ$	objc_type[1]= STAR $0.8'' < \delta < 10.0''$ [2]	537
Targeted WDs		STAR_WHITE_DWARF target flag set	1575
Princeton[4] WD or HOT Star	 $(u-g)_\circ < 0.90$ if —> (to exclude BHB)	spectrum classified as WD, DH, DQ OR as O, OB, B6, B9, A0, A0p by alternate pipeline at Princeton classified as B or A	4122
Eyeball		rejects from other searches with manual possible white dwarf ID made	1138

[1]objc_type is a *frames* pipeline output that does a simple star/galaxy separation. See http://www.sdss.org/dr1/algorithms/classify.html.

[2]δ is the difference between USNO-A catalog coordinates and SDSS observed coordinates, available in the USNO table in the SDSS databases. The timebase is about 50 years.

[3]H_g is the reduced proper motion: $H_g = g + 5 \times \log \mu + 5$ where μ is the proper motion in $''/yr$.

[4]D. Schlegel (private communication) has an independent spectroscopic pipeline, specBS, running at Princeton. This selection category uses results from that pipeline.

Table 3. SDSS DR1 spectroscopically identified DA stars.

Plate	MJD	Fiber	RA (deg)	Dec (deg)	u_{psf}	δ_u	S/N_g	PM_{RA} (mas yr^{-1})	PM_{Dec} (mas yr^{-1})	A_g	T_{eff} (K)	$\delta_{T_{eff}}$ (K)	log g	$\delta_{\log g}$	chi^2	AutoID	Notes
0651	52141	382	1.34173	−9.54185	20.30	0.06	3.61	18	−10	0.142	0	0	0.00	0.00	0.00	N/A	2
0388	51793	001	2.67918	−0.89987	19.41	0.03	5.78	−26	−12	0.154	0	0	0.00	0.00	0.00	N/A	2
0389	51795	431	3.41294	0.32358	15.76	0.02	70.39	398	−175	0.107	0	0	0.00	0.00	0.00	N/A	2
0366	52017	151	262.45991	58.30243	18.29	0.02	11.32	4	−8	0.159	90975	6897	7.71	0.39	1.01	DA0.6_7.7	
0494	51915	052	188.65494	66.72683	18.40	0.02	15.09	−1	−4	0.056	91304	6285	7.37	0.26	0.97	DA0.6_7.4	
0413	51929	483	49.74284	0.39049	17.91	0.02	16.89	3	−2	0.300	93855	5768	7.18	0.27	1.00	DA0.5_7.2	

Note. — Table 3 is published in its entirety in the electronic edition of the *Astrophysical Journal* and at the URL provided in the text. A portion is shown here for guidance regarding its form and content. The SDSS Object name, and the g,r,i,z magnitudes have been removed from this sample table which displays the data from the first and last three entries of the full table.

[1] Computer fit checked and found to be a reasonable fit.

[2] Computer fit checked and found not to be a believable fit.

[3] The computer fit may be affected by a late-type companion.

[4] This particular object is described further in the "Interesting Objects" section of the text.

[5] This object had no "best" photometry in the DR1 database, so the ugriz magnitudes come from the "target" photometry. (The lack of "best" photometry is probably due to the object being on the edge of the DR1 survey limits.)

[6] This DB spectrum also shows signs of Hydrogen.

[*] Magnitudes marked with an * have bad photometric pipeline quality control flags set.

Table 4. SDSS DR1 spectroscopically identified DB stars.

Plate	MJD	Fiber	RA (deg)	Dec (deg)	u_{psf}	δ_u	S/N_g	PM_{RA} (mas yr^{-1})	PM_{Dec} (mas yr^{-1})	A_g	T_{eff} (K)	$\delta_{T_{eff}}$ (K)	log g	$\delta_{\log g}$	chi^2	AutoID	Notes
0427	51900	320	29.12326	13.29576	*17.95	0.02	23.04	8	−4	0.211	0	0	0.00	0.00	0.00	N/A	2
0455	51909	247	38.38922	−9.39038	18.10	0.03	18.17	0	4	0.107	0	0	0.00	0.00	0.00	N/A	2
0464	51908	278	59.07291	−6.51934	18.68	0.02	16.23	13	17	0.287	0	0	0.00	0.00	0.00	N/A	2
0532	51993	358	210.49622	2.35743	18.73	0.03	10.41	−2	8	0.120	38211	1188	7.92	0.17	1.17	DB1.3_7.9	
0465	51910	518	62.22750	−4.56518	19.05	0.03	10.64	−3	−17	0.364	40000	1016	8.09	0.17	1.23	DB1.3_8.1:	4 6
0348	51671	003	249.65933	−0.90486	19.42	0.03	8.33	−1	−16	0.506	40000	317	7.05	0.06	1.45	DB1.3_7.1:	4 6

Note. — Table 4 is published in its entirety in the electronic edition of the *Astrophysical Journal* and at the URL provided in the text. A portion is shown here for guidance regarding its form and content. The SDSS Object name, and the g,r,i,z magnitudes have been removed from this sample table which displays the data from the first and last three entries of the full table.

[1] Computer fit checked and found to be a reasonable fit.

[2] Computer fit checked and found not to be a believable fit.

[3] The computer fit may be affected by a late-type companion.

[4] This particular object is described further in the "Interesting Objects" section of the text.

[5] This object had no "best" photometry in the DR1 database, so the ugriz magnitudes come from the "target" photometry. (The lack of "best" photometry is probably due to the object being on the edge of the DR1 survey limits.)

[6] This DB spectrum also shows signs of Hydrogen.

[*] Magnitudes marked with an * have bad photometric pipeline quality control flags set.

Table 5. All SDSS DR1 spectroscopically identified white dwarf and subdwarf stars.

Plate	MJD	Fiber	RA (deg)	Dec (deg)	Epoch	u_{psf}	δ_u	S/N_g	PM_{RA} (mas yr^{-1})	PM_{Dec} (mas yr^{-1})	A_g	Human ID	Notes
0650	52143	497	0.02983	−9.72773	2000.74	19.40	0.04	7.74	N/A	N/A	0.127	DA	
0650	52143	450	0.04820	−8.83566	2000.74	19.42	0.04	11.04	106	−2	0.140	DQ	
0650	52143	217	0.09390	−10.86172	2000.74	19.28	0.03	12.17	43	−27	0.131	DA5	
0386	51788	035	358.87400	−0.00391	2001.79	20.14	0.12	4.67	1	−2	0.150	DA	
0387	51791	347	359.22201	0.36072	2001.79	19.72	0.05	8.76	76	85	0.141	DA	
0650	52143	233	359.60751	−10.57039	2000.74	17.25	0.04	35.13	59	−21	0.122	DA	

Note. — Table 5 is published in its entirety in the electronic edition of the *Astrophysical Journal* and at the URL provided in the text. A portion is shown here for guidance regarding its form and content. The SDSS Object name, and the g,r,i,z magnitudes have been removed from this sample table which displays the data from the first and last three entries of the full table.

[1]Computer fit checked and found to be a reasonable fit.

[2]Computer fit checked and found not to be a believable fit.

[3]The computer fit may be affected by a late-type companion.

[4]This particular object is described further in the “Interesting Objects” section of the text.

[5]This object had no “best” photometry in the DR1 database, so the ugriz magnitudes come from the “target” photometry. (The lack of “best” photometry is probably due to the object being on the edge of the DR1 survey limits.)

[6]This DB spectrum also shows signs of Hydrogen.

[*]Magnitudes marked with an * have bad photometric pipeline quality control flags set.

Table 6. All SDSS DR1 spectroscopically identified white dwarf and subdwarf stars with uncertain identifications.

Plate	MJD	Fiber	RA (deg)	Dec (deg)	Epoch	u_{psf}	δ_u	S/N_g	PM_{RA} (mas yr^{-1})	PM_{Dec} (mas yr^{-1})	A_g	Human ID	Notes
0388	51793	350	1.29140	0.63600	2001.79	17.77	0.03	16.37	23	23	0.157	SDO:	
0417	51821	359	7.05945	15.02500	1999.78	20.84	0.08	2.94	N/A	N/A	0.246	DA:	
0417	51821	345	7.13435	15.23070	1999.78	20.59	0.07	4.45	N/A	N/A	0.254	SDB:	
0386	51788	403	357.27549	1.00614	2002.68	19.94	0.20	3.73	0	−16	0.097	DB:	
0386	51788	054	358.12767	−0.64107	2002.68	20.34	0.48	2.42	−5	−11	0.111	DA:	
0386	51788	110	358.59147	−0.35811	2002.68	20.71	0.19	3.77	2	−8	0.116	DA:	

Note. — Table 6 is published in its entirety in the electronic edition of the *Astrophysical Journal* and at the URL provided in the text. A portion is shown here for guidance regarding its form and content. The SDSS Object name, and the g,r,i,z magnitudes have been removed from this sample table which displays the data from the first and last three entries of the full table.

[1]Computer fit checked and found to be a reasonable fit.

[2]Computer fit checked and found not to be a believable fit.

[3]The computer fit may be affected by a late-type companion.

[4]This particular object is described further in the "Interesting Objects" section of the text.

[5]This object had no "best" photometry in the DR1 database, so the ugriz magnitudes come from the "target" photometry. (The lack of "best" photometry is probably due to the object being on the edge of the DR1 survey limits.)

[6]This DB spectrum also shows signs of Hydrogen.

[*]Magnitudes marked with an * have bad photometric pipeline quality control flags set.

Table 7. SDSS photometric pipeline output flags used to indicate bad photometry.

Flag	Description
EDGE	object too close to edge of frame to be measured
PEAKCENTER	used brightest pixel as centroid
NOPROFILE	only 0 or 1 entries for the radial flux profile
BAD_COUNTS_ERROR	interpolation affected many pixels
INTERP_CENTER	interpolated pixel(s) within 3 pixels of the center
	(we only use this flag if a cosmic ray was flagged as well)
DEBLEND_NOPEAK	object is a CHILD of a DEBLEND but has no peak
	(we only use this flag if the PSF magnitude error > 0.2 mag)
PSF_FLUX_INTERP	more than 20% of PSF flux is interpolated over
SATUR	contains saturated pixels
NOTCHECKED	object contains pixels which were not checked for peaks by deblender

Table 8. Multiplicative conversion values, N, to go from A_g to the extinction in any other SDSS filter. $A_x = N * A_g$.

Filter	N
u	1.360
g	1.000
r	0.726
i	0.550
z	0.390

Table 9. Fitted DAs with measured log g values between 6.7 to 7.0.

Name	log g	$T_{\rm eff}$
SDSS J123410.37–022802.9	6.34 ± 0.05	17308 ± 226
SDSS J234536.48–010204.8	6.74 ± 0.23	33049 ± 1105
SDSS J002207.65–101423.5	6.82 ± 0.16	19672 ± 729
SDSS J105611.03+653631.5	6.97 ± 0.12	20290 ± 637
SDSS J131033.26+644032.9	6.97 ± 0.10	39937 ± 918
SDSS J142601.48+010000.2	6.97 ± 0.09	16465 ± 355
SDSS J163800.36+004717.8	6.98 ± 0.23	73256 ± 4366

Table 10. The best examples of fitted DAs with likely high log g values above 8.5.

Name	log g	$T_{\rm eff}$
SDSS J144707.42+585506.7	8.94 ± 0.06	14802 ± 439
SDSS J024700.48–070547.1	8.97 ± 0.04	19866 ± 791
SDSS J113509.97+642949.0	8.98 ± 0.03	9031 ± 34
SDSS J002049.39+004435.1	9.00 ± 0.00	9182 ± 17
SDSS J011055.07+143922.3	9.00 ± 0.00	9406 ± 18
SDSS J020626.89–005710.0	9.00 ± 0.01	7841 ± 37
SDSS J075916.54+433519.1	9.00 ± 0.00	22222 ± 392
SDSS J155238.21+003910.4	9.00 ± 0.00	16981 ± 441

Note. — The clustering of log g around 9.0 (with small errors) is an artifact of our limited model grid and our fitting technique at the limits of our grid. The true log g values are likely high, but may not be exactly as determined here.

Table 11. Previously known white dwarf stars recovered in this work.

SDSS Name	g_{psf}	SDSS Type	Other Name	Other Type	Note
SDSS J001339.11+001924.9	15.37	DA5.3:	WD0011+000	DA6	1
SDSS J002602.29–103752.0	16.22	DA5.0:	WD0023–109	DA7	1
SDSS J003230.11+001138.4	18.64	DB3.7:	WD0029–000	DB	
SDSS J003508.26+135045.3	16.37	DA2.3:	HS0032+1334	DA	2
SDSS J003426.93+151801.8	16.99	DA6.6:	WD0031+150	DA7	
SDSS J004022.88–002130.1	14.83	DA3.3:	WD0037–006	DA4	1
SDSS J010207.17–003259.5	18.21	DA4.6	WD0059+002	DA	
SDSS J011009.10+132616.1	16.54	DAMe	HS0107+1310	DA	2
SDSS J011055.07+143922.3	16.91	DA5.3	WD0108+143	DA	1
SDSS J021028.69+124319.0	16.86	DA3.0:	HS0207+1229	DA	2
SDSS J024602.67+002539.3	17.21	DA3.5:	WD0243+002	DA	1
SDSS J024821.95+005109.1	17.99	DA3.3	WD0245+006	DA	
SDSS J025200.98+004544.2	18.41	DA4.9	WD0249+005	DA	1
SDSS J025624.74+003558.0	18.07	DA1.3	WD0253+003	DA	
SDSS J025709.00+004628.1	17.38	DA4.1	WD0254+005	DA	
SDSS J025746.41+010106.0	17.66	DA3.0	WD0255+008	DA	
SDSS J025801.20–005400.1	18.03	DA5.3	WD0255–010	DA	
SDSS J025817.87+010946.0	18.20	DAM	WD0255+009.2	DA	
SDSS J030407.40–002541.7	17.75	DAH	WD0301–006	DAH3.4	3
SDSS J031305.82–070749.5	16.47	DA2.8	WD0310–073	DA	
SDSS J032302.85+000559.7	17.44	DA3.8	WD0320–000	DA	
SDSS J033133.89+010327.9	16.43	DA1.4:	WD0328+008	DA	
SDSS J033145.69+004517.0	17.21	DAH	WD0329+005	DAH	
SDSS J033200.49–005752.5	17.07	DA2.9	WD0329–011	DA	
SDSS J033320.37+000720.7	16.53	DBH	WD0330–000	DB:HP	
SDSS J034511.11+003444.3	18.63	DH	WD0342+004	DAH6.3	3
SDSS J075723.93+400714.8	17.55	DA2.6	WD0754+402	DA	
SDSS J075959.56+433521.3	16.19	DAH	WD0756+437	DAH	1
SDSS J080459.02+415744.9	17.45	DA3.6	WD0801+421	DA	
SDSS J084951.11+553514.7	16.20	DA1.8:	WD0846+557	DA2	
SDSS J093958.66+011638.2	16.45	DA2.6:	HS0937+0130	DA	2
SDSS J094640.35+011319.9	17.18	DA2.5:	HS0944+0127	DA	2
SDSS J095102.23+010432.6	15.59	DB2.9:	WD0948+013	DB2	

Table 11—Continued

SDSS Name	g_{psf}	SDSS Type	Other Name	Other Type	Note
SDSS J095220.45+005913.2	18.96	DA4.8	WD0949+012	DA5.0	
SDSS J095245.59+020938.9	16.35	DA1.2:	WD0950+023	DA1	1
SDSS J095810.68–010417.8	16.51	DA2.1:	WD0955–008	DA2	
SDSS J100316.35–002337.0	15.96	DA2.5:	WD1000–001	DA2.5	
SDSS J101219.90+004019.7	17.72	DQ	WD1009+009	DC	1
SDSS J101232.49+015444.6	18.04	DA2.2:	WD1009+021	DA2.0	
SDSS J101548.01+030648.4	15.66	DA4.3:	HS1013+0321	DA	2
SDSS J101607.40+002038.2	18.71	DA2.5	WD1013+005	DA2.5	
SDSS J101805.04+011123.5	16.29	DAH	WD1015+014	DAP3.5	
SDSS J102549.72+003906.2	16.07	DA1.4:	WD1023+009	DA1.5	1
SDSS J102732.54–005440.1	18.76	DA2.0	WD1024–006	DA2.5	
SDSS J103004.51–010919.1	18.71	DA1.9:	WD1027–008	DA2.0	
SDSS J103448.94+005201.3	19.08	DA5.2:	WD1032+011	DA3.0	
SDSS J103635.66–000036.4	18.92	DA3.6:	WD1034+002	DA3.5	
SDSS J104946.47+003635.1	17.25	DA2.2	HS1047+0052	DA	2
SDSS J110515.32+001626.1	15.20	DA3.9:	HS1102+0032	DA	2
SDSS J110636.72–001122.4	18.32	DA3.3	WD1104+000	DA3.5	
SDSS J111028.70–003343.5	18.61	DA5.2:	WD1107–002	DA5.0	
SDSS J113901.22+000321.8	18.87	DA3.7	WD1136+003	DA3.0	
SDSS J114312.57+000926.5	18.15	DAM	WD1140+004	DA4.0+M	
SDSS J114425.06+013949.4	18.19	DA4.0	WD1141+019	DA	
SDSS J114635.23+001233.4	14.88	PG1159	WD1144+004	DQZO1	
SDSS J114913.53–014728.6	17.98	DAM	WD1146–015	DA	1
SDSS J115418.14+011711.4	17.75	DAH	HS1151+0133	DA	2
SDSS J121635.37–002656.2	19.60	DAH	WD1214–001	DAH	3
SDSS J122209.44+001534.0	20.27	DAH	SDSS J1222	DAH	3
SDSS J123706.24–001603.9	19.05	DA3.1	WD1234+000	DA3.5	
SDSS J123819.77+005248.2	18.91	DA5.6	WD1235+011	DA	
SDSS J123836.35–004042.3	17.41	DAM	WD1236–004	DA	
SDSS J123836.74–013936.2	18.84	DA3.2	WD1236–013	DA	1
SDSS J123910.18–010005.4	19.08	DA1.9	WD1236–007	DA	1
SDSS J123922.34+005548.8	19.27	DAM	WD1236+012	DA3.0+M	
SDSS J124438.81–022107.5	18.39	DA4.6	WD1242–020	DA3.5	

Table 11—Continued

SDSS Name	g_{psf}	SDSS Type	Other Name	Other Type	Note
SDSS J124709.83+005533.0	19.37	DA2.7	WD1244+011	DA4.0	
SDSS J124920.09+001911.6	19.73	DA2.2:	WD1246+005	DA2.5	
SDSS J125139.78–010254.1	18.38	DA4.9	WD1249–007	DA3.0	
SDSS J125730.31–001150.9	18.79	DA1.7	WD1254+000	DA1.5	
SDSS J130110.51+010739.9	16.30	DA4.5	WD1258+013	DA	
SDSS J130815.22–015904.5	16.80	DA0.9	WD1305–017	DAO1	1
SDSS J131717.02–021945.6	18.32	DB2.8	WD1314–020	DB	
SDSS J131724.75+000237.4	15.77	DO	WD1314+003	DO	
SDSS J132232.12+641545.8	16.25	DA1.8:	WD1320+645	DA2	1
SDSS J132439.71–031923.5	18.15	DA3.5	WD1322–030	DA	1
SDSS J133137.06+010632.1	17.43	DA1.4	HS1329+0121	DA	2
SDSS J133739.40+000142.9	19.57	DC	WD1335+002	DC	4
SDSS J133838.48–000712.4	18.70	DA4.9	WD1336+001	DA3.0	
SDSS J134430.11+032423.2	16.61	DA3.7:	HS1341+0339	DA	2
SDSS J135211.00+652457.1	15.44	DA4.2:	WD1350+656	DAV4.2	
SDSS J135459.89+010819.3	16.36	DA4.3:	HS1352+0123	DA	2
SDSS J135532.42+001124.0	15.71	DB3.2:	WD1352+004	DB4	
SDSS J141011.44+045255.8	17.40	DA3.4	HS1407+0507	DA	2
SDSS J141457.89+012207.4	17.83	DA5.5:	HS1412+0136	DA	2
SDSS J143947.62–010606.9	16.52	DAMe	WD1437–008	DC	
SDSS J144433.80–005958.9	16.22	DA4.0	WD1441–007	DA3	
SDSS J144518.03+585032.2	17.70	DBZ	WD1443+590	DB	
SDSS J144828.21–010525.5	18.87	DA3.8	WD1445–008	DA3.5	
SDSS J145535.49+010246.5	18.95	DA5.4	WD1453+012	...	
SDSS J145600.81+574150.8	16.19	DA1.6:	WD1454+578	DA	
SDSS J145644.91+011017.6	19.05	DB3.1	WD1454+013	...	
SDSS J145947.04–003954.6	18.40	DB3.0:	WD1457–004	...	
SDSS J150003.86+002420.0	18.80	DB3.4	WD1457+006	...	
SDSS J150231.66+011045.9	18.47	DAM	WD1459+013	...	
SDSS J150547.49+024840.6	16.34	DA2.8	HS1503+0300	DA	2
SDSS J151151.36+562450.5	16.31	DA5.5	WD1510+566	DA6	1
SDSS J151421.26+004752.8	15.68	DA1.8	WD1511+009	DA2	
SDSS J152839.42+011300.1	16.45	DA0.9	WD1526+013	DA1	

Table 11—Continued

SDSS Name	g_{psf}	SDSS Type	Other Name	Other Type	Note
SDSS J154338.69+001202.1	16.76	sdB	WD1541+003	DAwk	1
SDSS J165401.26+625355.0	18.40	DC	WD1653+630	DC9	
SDSS J165935.58+620933.9	16.25	DA4.1	WD1659+622	DA	
SDSS J172045.37+561214.9	20.10	DAH	WD1719+562	DAH	3
SDSS J172329.14+540755.8	18.78	DAH	WD1722+541	DAH3.1	3
SDSS J172643.38+583732.2	15.32	DA0.8:	WD1725+586	DA	1
SDSS J172856.22+555822.8	15.98	DQABCI	WD1727+560	DQAB?4	
SDSS J232248.22+003900.9	19.14	DAH	WD2320+003	DAH1.3	3
SDSS J232337.55–004628.2	17.98	DBH	WD2321–010	DAH?2.5	3
SDSS J235410.39–010728.5	18.19	DB3.5:	WD2351–014	DB	1

[1]SDSS position different from previous by more than 10 arcsec.

[2]Unpublished white dwarf, in Hamburg Quasar Survey (Homeier 2002, priv. comm.).

[3]White dwarf discovered in the SDSS EDR (Gansicke et al. 2002).

[4]White dwarf discovered in the SDSS (Harris et al. 2001).

Table 12. Previously known white dwarf stars not spectroscopically recovered in this work.

Name	Type	Mag	RA (J2000)	Dec (J2000)	u_{psf}	δ_u	Notes
WD0041–102	DBAP3	14.47 v	00 43 45.98	–10 00 25.1	14.25	0.01	
WD0042+140	DC:	18.9 p	00 45 25.79	+14 21 29.4	22.00	0.25	
WD0106–109.1	DA	16.5 p	01 09 03.43	–10 42 14.2	17.15	0.02	
WD2318+007.1	DC:	18.8 p	23 21 15.32	+01 02 11.3	20.53	0.10	
WD2318+007.2	DC:	19.7 p	23 21 15.68	+01 02 23.9	21.70	0.26	
WD2333–002	DA2?	15.49 p	23 35 41.47	+00 02 19.5	15.30	0.02	

Note. — Table 12 is published in its entirety in the electronic edition of the *Astrophysical Journal* and at the URL provided in the text. A portion is shown here for guidance regarding its form and content. The SDSS g,r,i,z magnitudes have been removed from this sample table which displays the data from the first and last three entries of the full table.

[*]Star image contains saturated pixels in this filter.

[1]No white dwarf found near this position.

[2]SDSS spectrum 0410–51816–565 shows WD0255+009.1 is a QSO.

[3]No SDSS imaging data, too near bright star.

[4]Probably same star as WD0330–009.

[5]WD0820+021 probably not detected, too faint.

[6]Spectrum not in DR1, but is given in Initial Survey paper (Harris et al. 2003).

[7]Falls in small gap in SDSS imaging data.

[8]Unresolved with WD1330+015.1.

[9]The colors of WD1401+005 are red and indicate it is not a white dwarf.

[10]Probably same star as WD1422+028.

[11]Colors are very red and indicate WD1449+003 is not a white dwarf.

[12]Colors indicate WD1451–004, WD1455+019, and WD1500+006 are horizontal-branch stars, not white dwarf stars.

[13]Probably same star as WD1544+009.